# Design of a bistable switch to control cellular uptake

Diego A. Oyarzún[1] and Madalena Chaves[2]

[1] Department of Mathematics, Imperial College London
London, SW7 2AZ, United Kingdom
✉ d.oyarzun@imperial.ac.uk
[2] BioCore team, INRIA Sophia Antipolis
2004 Route des Lucioles, BP 93, 06902, Sophia Antipolis, France

**Abstract**

Bistable switches are widely used in synthetic biology to trigger cellular functions in response to environmental signals. All bistable switches developed so far, however, control the expression of target genes without access to other layers of the cellular machinery. Here we propose a bistable switch to control the rate at which cells take up a metabolite from the environment. An uptake switch would provide a new interface to command metabolic activity from the extracellular space and has great potential as a building block in more complex circuits that coordinate pathway activity across cell cultures, allocate metabolic tasks among different strains, or require cell-to-cell communication with metabolic signals. Inspired by uptake systems found in nature, we propose to couple metabolite import and utilization with a genetic circuit under feedback regulation. Using mathematical models and analysis, we determined the circuit architectures that produce bistability and obtained their design space for bistability in terms of experimentally tuneable parameters. We found an Activation-Repression architecture to be the most robust switch because it displays bistability for the largest range of design parameters and requires little fine-tuning of the promoters' response curves. Our analytic results are based on on-off approximations of promoter activity and are in excellent qualitative agreement with simulations of more realistic models. With further analysis and simulation, we established conditions to maximise the parameter design space and to produce bimodal phenotypes via hysteresis and cell-to-cell variability. Our results highlight how mathematical analysis can drive the discovery of new circuits for Synthetic Biology, as the proposed circuit has all the hallmarks of a toggle switch and stands as a promising design to control metabolic phenotypes across cell cultures.

**Keywords —** synthetic biology; genetic circuits; bistability; cellular uptake; dynamic metabolic engineering; piecewise affine models

# 1 Introduction

Bistable switches are ubiquitous components in natural and engineered biological systems. They play a key role in controlling cellular decisions [1, 2] and are common building blocks in synthetic gene circuits [3, 4, 5, 6]. The aim of all synthetic switches developed so far has been to produce bistable expression of target genes. One of the major goals in synthetic biology, however, is to scale up biomolecular circuits to systems that interface gene circuits with metabolic activity. These have great potential to expand the functionality of biomolecular devices, for example, to dynamically reroute flux through heterologous pathways [7] or to design self-adaptive pathways in metabolic engineering [8, 9, 10].

The "metabolator", a genetic circuit designed to generate an oscillatory metabolic flux [11], showcased how complex responses could be engineered by coupling the genetic and metabolic machinery. To date, however, little progress has been made in engineering other metabolic phenotypes. A bistable uptake switch has been particularly elusive, although it is a key building block for more complex circuits that require metabolic control with extracellular metabolites. An uptake switch can be used to coordinate pathway activity in multicellular systems, for example, by allocating metabolic tasks among several strains [12] or by acting as a communication device via metabolic signals [13]. In microbial consortia, an uptake switch can control the division of labor through diversified phenotypes of slow- and fast-feeders. Bistable uptake can also serve as mechanism to engineer bacterial bet-hedging that favours survival in adverse environments [14, 15] or as a research tool to study cellular adaptation strategies [16], e.g. in competition assays where subpopulations of switchers and non-switchers adapt to limited carbon sources or fluctuations in nutrient abundance.

Metabolic uptake is typically carried out by transport enzymes in the cell membrane, but their kinetics do not naturally display bistability (Fig. 1A). Although ultrasensitive kinetics [17] can generate a switch-like response in the uptake rate, or even generate bistability through covalent modifications [18], tuneable implementations of such such kinetic mechanisms require protein engineering beyond our current capabilities.

In this paper we propose a bistable switch to control the rate at which cells take up a metabolite from the environment. We identify a genetic-metabolic system that reversibly toggles between slow and fast uptake in response to the amount of metabolite in the extracellular space. Our design relies on coupling enzyme activity with a gene regulatory circuit designed to shape the uptake response as a bistable switch. We borrowed this strategy from two well known

bistable uptake systems found in nature: the lactose operon in *E. coli* [19] and the galactose pathway in *S. cerevisiae* [14, 20]. Both systems produce bistability through an underlying gene regulatory network that controls the expression of key enzymes.

We consider uptake circuits based on feedback regulation of the expression of transport and utilization enzymes (Fig. 1B). The circuit architecture requires two metabolite-responsive promoters and includes four regulatory motifs depending on whether the internalized metabolite activates or represses enzyme expression (Fig. 1C). Two of these motifs can be found in natural and engineered systems. The Activation-Activation circuit (labelled AA in Fig. 1C) has a similar architecture as the lactose operon [19], where an intracellular metabolite (allolactose) upregulates a transporter and a metabolic enzyme through binding to a transcriptional repressor. A Repression-Activation circuit (RA), on the other hand, has been used to improve the production of fatty acids by balancing the supply and consumption of the intermediate malonyl-CoA [10].

From a general model for the uptake circuits, we identified those that produce bistability and determined analytic conditions for bistability in terms of the promoters' dynamic ranges and transcriptional thresholds. Our approach combines a qualitative on-off model for promoter activity together with a separation of timescales [21]. This leads to a reduced model based on piecewise affine differential equations where bistability can be studied analytically [22]. The analysis revealed that the circuits have a rich diversity of *bistable regimes*, i.e. qualitatively different combinations of stable steady states that lead to a bistable uptake flux, all of which can be linked to different *design spaces* for the promoter parameters. The multiple number of bistable regimes contrasts with, for example, the original genetic toggle switch that has only one regime for bistability [3]. Our analysis method relies on a coarse approximation of the true system dynamics, but uncovers useful relations between experimentally tuneable parameters and the resulting metabolic phenotypes. We used the derived conditions to distinguish the bistable regimes via the shape and size of their design spaces [23]. With the size of the design space as a proxy for robustness, we found that the Activation-Repression circuit (AR) is the best candidate for an uptake switch, as it displays bistability for a large range of promoter dynamic ranges and therefore it is likely to be more robust in face of cell-to-cell variability and unreliable estimates for the enzyme kinetic parameters. Further analyses of the AR system revealed analytic conditions for hysteresis and design rules to maximise the promoter design space with the transcriptional thresholds. We validated our results and the performance of the AR circuit with extensive simulations of a more realistic, continuous, model for promoter activity. Population-

wide simulations show that the circuit diversifies the uptake phenotypes by splitting a culture into two subpopulations with slow and fast uptake.

Our study puts forward the AR circuit as a promising design for an uptake switch in future synthetic biology applications that require metabolic control across cell cultures. A key challenge in the implementation of the uptake switch is the lack of intracellular sensors that interface metabolic signals with gene expression. This limitation is not specific to our study and pervades all current efforts to engineer genetic-metabolic circuits [24, 25]. Successful implementations have relied on metabolite-responsive promoters [8, 10, 11], but the design and construction of such sensing mechanisms requires a substantial amount of experimental work. Our study demonstrates how mathematical design can be an effective tool to identify circuit architectures for a new biological function and to single out the key design parameters that need to be tuned, both of which can help to focus and accelerate the experimental work in the field.

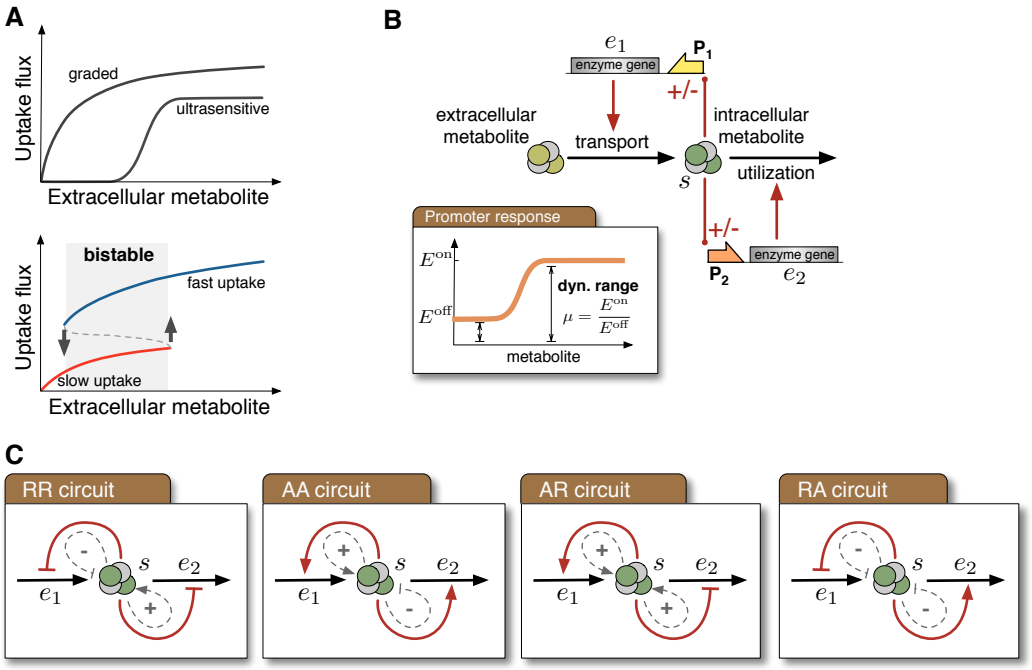


**Figure 1** – Bistable switches for cellular uptake with a two-promoter circuit under feedback regulation. (**A**) Graded, ultrasensitive and bistable uptake. A bistable system switches between slow and fast uptake, and displays hysteresis because of different switching points. (**B**) Circuit architecture for the uptake systems: a transport enzyme ($e_1$) imports a metabolite into the intracellular space. A second enzyme ($e_2$) metabolizes the internalized metabolite ($s$). The circuit contains two promoters ($P_1$ and $P_2$) that control enzyme expression through feedback from the intracellular metabolite, including four combinations of (A)ctivation and (R)epression feedback loops; the main design parameters are the dynamic ranges $\mu$ of both promoters, defined as the ratio between maximal and baseline expression levels (see inset). (**C**) Schematics for the four uptake circuits. Each circuit has two interlinked positive and negative feedback loops (shown in dashed lines); a faster utilization causes a decrease in the concentration of metabolite, and thus upregulation (downregulation) of the utilization enzyme corresponds to negative (positive) feedback.

## 2 General model for synthetic uptake circuits

We consider uptake circuits composed of two enzymes and an internalized metabolite ($s$) as illustrated in Fig. 1B. A transport enzyme ($e_1$) imports the extracellular metabolite ($s_0$) into the cell, which is then metabolized by different cellular processes represented by an utilization enzyme ($e_2$). The network has two independent promoters that control the expression of enzymes in response to the internalized metabolite, thus forming two coupled feedback loops. We assume

that the extracellular metabolite concentration is constant so that the circuits are thermodynamically open and sustain a nonzero flux. We model the dynamics of the metabolite and enzymes as

$$\frac{\mathrm{d}s}{\mathrm{d}t} = g_1(s_0)e_1 - g_2(s)e_2, \tag{1}$$

$$\begin{aligned}\frac{\mathrm{d}e_1}{\mathrm{d}t} &= \kappa_1^0 + \kappa_1^1\sigma_1(s) - \gamma_1 e_1,\\ \frac{\mathrm{d}e_2}{\mathrm{d}t} &= \kappa_2^0 + \kappa_2^1\sigma_2(s) - \gamma_2 e_2,\end{aligned} \tag{2}$$

where $(s, e_1, e_2)$ are the species concentrations, $(\kappa_i^0, \kappa_i^1)$ are the baseline and induced enzyme expression rates, and $\gamma_i$ is a first order kinetic rate that accounts for protein degradation and dilution by cell growth.

The functions $g_i$ in equation (1) are the enzyme turnover rates, i.e. the reaction rate per unit of enzyme, and describe their kinetics for different substrate concentrations. We focus our analysis on a broad class of kinetic rate functions that includes the common Michaelis-Menten kinetics as a special case. To this end, we assume that the turnover rates are increasing functions of their substrate, so that $\mathrm{d}g_i(x)/\mathrm{d}x > 0$ with a saturation value $g_i^{\text{sat}} = \lim_{x\to\infty} g_i(x) = \sup g_i$. In the case of Michaelis-Menten kinetics, the turnover rate is $g(x) = k_{\text{cat}}\, x/(K_{\text{M}} + x)$ and has a saturation value $g^{\text{sat}} = k_{\text{cat}}$.

The enzyme equations in (2) describe the balance between protein synthesis and degradation. The functions $\sigma_i(s)$ are lumped models for the promoter response curves and describe the activation/repression of transcriptional activity by the internalized metabolite. We assume that the promoter response curves satisfy $\mathrm{d}\sigma_i/\mathrm{d}s > 0$, $\sigma_i(0) = 0$ and $\sigma_i(\infty) = 1$ in case of activation (conversely, $\mathrm{d}\sigma_i/\mathrm{d}s < 0$, $\sigma_i(0) = 1$ and $\sigma_i(\infty) = 0$ in case of repression). The promoters therefore control the enzymes between a baseline ("off") and a maximal concentration ("on"):

$$E_i^{\text{off}} = \frac{\kappa_i^0}{\gamma_i}, \quad E_i^{\text{on}} = \frac{\kappa_i^0 + \kappa_i^1}{\gamma_i}. \tag{3}$$

Promoter strengths are key parameters in promoter engineering [26] and one of the most easily tuneable parameters in synthetic circuits. Here we quantify the strength of promoters via their

*dynamic range* ($\mu_i$), i.e. the ratio between their maximal and baseline activity levels:

$$\mu_i = \frac{E_i^{\text{on}}}{E_i^{\text{off}}} = \frac{\kappa_i^0 + \kappa_i^1}{\kappa_i^0}. \tag{4}$$

As we shall see in the next section, we found that bistability depends critically on an additional design parameter, the *relative dynamic range* ($\mu_{12}$):

$$\mu_{12} = \frac{E_2^{\text{on}}}{E_1^{\text{off}}} = \frac{\kappa_2^0 + \kappa_2^1}{\kappa_1^0}\frac{\gamma_1}{\gamma_2}, \tag{5}$$

which corresponds to the maximal level of the utilization enzyme relative to the baseline level of the transport enzyme. We note that because the functions $\sigma_i$ lump transcription and translation together, our model can also account for the strength of ribosomal binding sites, another common tuneable parameter in gene circuits [27], via a linear scaling factor of enzyme expression rates in equation (2).

As shown in Fig. 1C, the general circuit architecture includes four uptake circuits, which we call AA, RR, AR, and RA depending on the particular combination of gene (A)ctivation or (R)epression. Each network can can be seen as combinations of two interlinked positive and negative feedback loops. In particular, we can readily rule out bistability in the RA network because it does not contain any positive feedback loop, a well-known necessary condition for bistability [28]. In the next section we will determine conditions under which the other three circuits in Fig. 1C display two steady state fluxes.

## 3 Bistability in the synthetic uptake circuits

The steady state uptake flux in the circuits is

$$J = g_1(s_0)\bar{e}_1 = g_2(\bar{s})\bar{e}_2, \tag{6}$$

where the bars denote steady state concentrations. The steady state transport flux depends only on the concentration of the transport enzyme ($e_1$). The utilization reaction, in contrast, depends on both the metabolite and enzyme, and therefore different steady state concentrations can lead to the same utilization flux. For example, in equation (6) a slow utilization flux can be sustained by a lowly abundant metabolite and an overexpressed utilization enzyme, or a highly abundant

metabolite and an underexpressed utilization enzyme. These two scenarios require promoters to operate at different activity levels and lead to steady states that are qualitatively different. Next we will show that a single uptake circuit can display a number of *bistable regimes*, i.e. qualitatively different combinations of steady state concentrations that lead to a bistable flux. We will then provide analytic conditions that describe all combinations of promoter dynamic ranges that produce bistability, which we will refer to as the *promoter design space*.

### 3.1 Identification of all bistable regimes

Using the model in (1)–(2) we can obtain an equation for the steady state metabolite concentration:

$$g_2(\bar{s}) = g_1(s_0)\left(\frac{\kappa_1^0 + \kappa_1^1\sigma_1(\bar{s})}{\kappa_2^0 + \kappa_2^1\sigma_2(\bar{s})}\right)\frac{\gamma_2}{\gamma_1}, \tag{7}$$

from where both enzyme concentrations can be computed as $\bar{e}_i = \left(\kappa_i^0 + \kappa_i^1\sigma_i(\bar{s})\right)/\gamma_i$. The ideal would be to have analytic solutions of (7) that show how bistability depends on the promoter dynamic ranges, potentially revealing structural differences among the circuits. However, the steady state equation is analytically intractable because of the nonlinearities in the enzyme kinetics ($g_2$) and promoter response curves ($\sigma_i$). For some parameter combinations, the circuits may also lead to unbounded accumulation of the metabolite due to saturation of the utilization enzyme. This happens when the steady state equation does not have a solution because the right hand side of (7) is higher than the saturation value of $g_2$.

In general, the number of steady states and their stability depend intricately on the model parameters and the shape of the nonlinearities. A common strategy to detect bistability is to use phase plane analysis to identify the number of steady state solutions and their behaviour with respect to model parameters. This approach becomes cumbersome in highly nonlinear models and requires case-by-case analyses for each uptake circuit. An alternative is to solve the steady state equation numerically for many parameter combinations and use linear stability analysis in each solution, or to run long model simulations for many initial conditions and single out those that lead to two final states. It is generally difficult, however, to establish whether bistability properties found with numerical search are structural features of the model, or if instead they are a consequence of the form of the nonlinearities and the specific choice for parameter values.

We can avoid the above difficulties with an analysis technique based on piecewise affine

models for gene regulation [22, 29] and a separation of timescales [21, 30]. This approach leads to a reduced model in which we can study bistability analytically. To obtain a tractable model, we assume that promoters switch between "on" and "off" activity levels depending on the amount of metabolite:

$$\underline{\text{Activation}} \qquad \bar{\sigma}_i(s) = \begin{cases} 0, & s < \theta_i, \\ 1, & s > \theta_i. \end{cases} \qquad\qquad \underline{\text{Repression}} \qquad \bar{\sigma}_i(s) = \begin{cases} 1, & s < \theta_i, \\ 0, & s > \theta_i. \end{cases} \tag{8}$$

where $\theta_i$ is a threshold for transcriptional activation or repression. Enzymatic catalysis occurs in a much faster time scale than enzyme expression, with kinetic time constants typically in the millisecond range [31] and gene expression in the order of tens of minutes or longer. We incorporated this timescale separation to obtain a reduced model that can be extensively analyzed in terms of its bistability properties.

Our analysis revealed that the uptake circuits can sustain a rich variety of bistable regimes. The results, summarized in Fig. 2 (details in Appendix A.1 and the Supplementary Material), indicate a total of nine qualitatively different regimes: one for the RR circuit, three for the AA circuit, and five for the AR circuit.

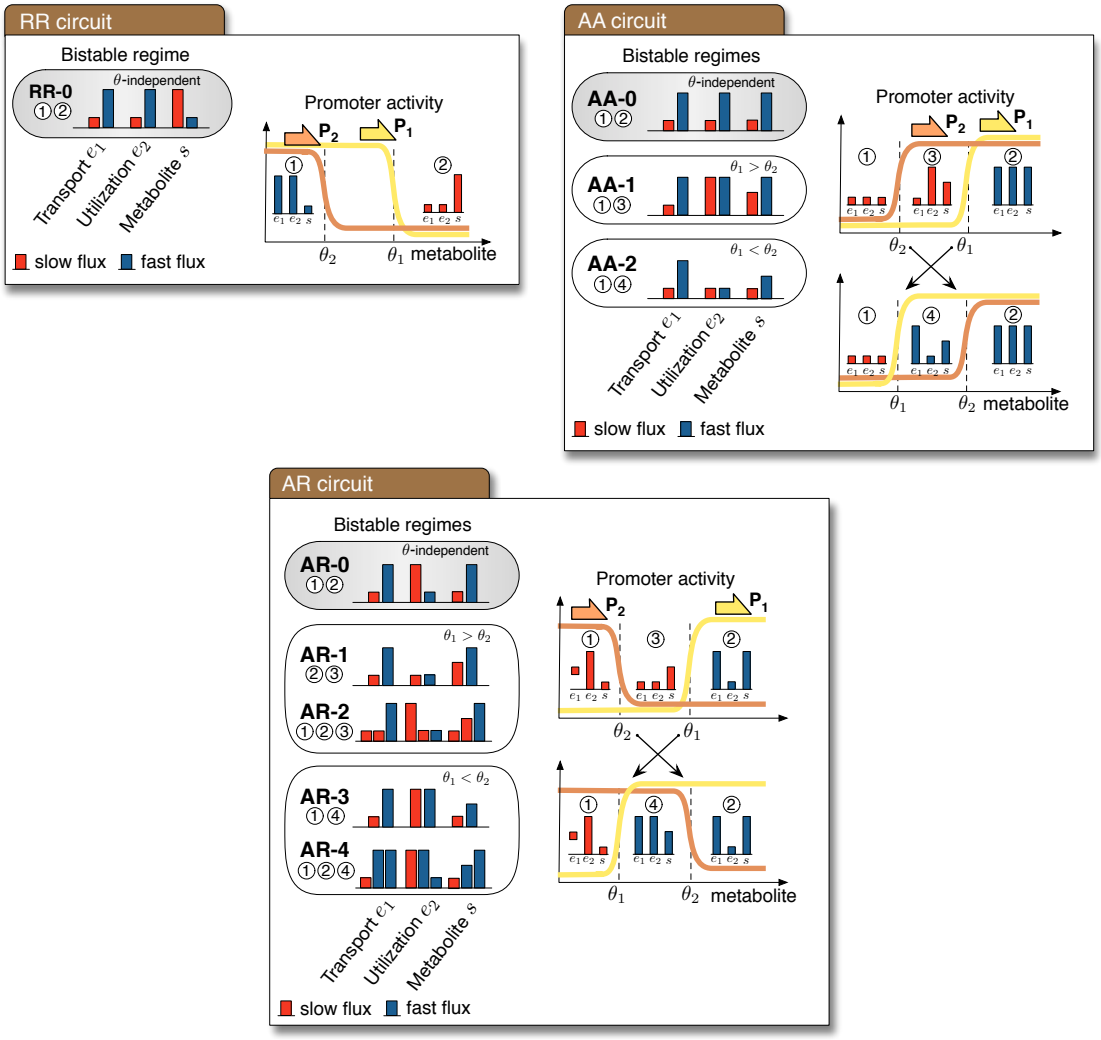


**Figure 2** – Bistable regimes in the uptake circuits. The bar plots (left panels) show all the qualitatively different regimes that sustain a bistable uptake flux. Each bistable regime corresponds to a combination of steady state concentrations from the right panels, marked with circled numbers. The steady state flux is proportional to the concentration of transporter enzyme, as shown in equation (6); therefore, low or high concentration of transporter ($e_1$) correspond to slow or fast uptake flux, respectively. For the enzymes, the bar height represents a baseline ($E_i^{\text{off}}$) or maximal ($E_i^{\text{on}}$) steady state concentration; for the metabolite, the bar height represents the qualitative steady state concentration of metabolite relative to the thresholds: e.g. if $\theta_2 < \theta_1$, the bars denote a low ($\bar{s} < \theta_2$), intermediate ($\theta_2 < \bar{s} < \theta_1$) or high ($\bar{s} > \theta_1$) concentration. The threshold-independent regimes (highlighted in gray) exist for any combination of regulatory thresholds. All the threshold-dependent regimes are sustained by an intermediate concentration of metabolite; these regimes vanish if both promoters have similar thresholds. The bistable regimes can be verified through numerical simulation of a continuous model with promoter responses described by steep sigmoids. Details on how to find the bistable regimes can be found in Appendix A.1 and the Supplementary Material.

As shown in Fig. 2, each bistable regime requires the promoters to operate at different activity levels depending on the steady state concentration of metabolite. Moreover, if promoters respond at different regulatory thresholds, the circuits can reach steady states with intermediate metabolite concentrations (i.e. $\theta_1 < \bar{s} < \theta_2$). As a consequence, the bistable regimes depend strongly on the promoter thresholds: we observe three threshold-independent regimes (RR-0, AA-0, and AR-0 in Fig. 2) and six threshold-dependent regimes that emerge depending on whether $\theta_1 < \theta_2$ or $\theta_1 > \theta_2$. The threshold-dependent regimes vanish when both promoters have similar thresholds. The results in Fig. 2 also uncover several qualitative differences among the circuits:

- The RR circuit has only one bistable regime. The circuit cannot reach an intermediate concentration of metabolite because this would cause transport to be too fast to be matched by a slow utilization (in the case $\theta_1 > \theta_2$), or too slow to be matched by a fast utilization (in the case $\theta_1 < \theta_2$). Such imbalance would ultimately lead to accumulation or depletion of the internalised metabolite.

- The AA and AR circuits, in contrast, admit intermediate steady state metabolite concentration, and consequently they can display two additional bistable regimes each (AA-1 and AA-2, AR-1 and AR-3, respectively).

- The AR circuit has two extra bistable regimes (AR-2 and AR-4) sustained by three stable steady states. We note that in these regimes, the three stable steady state concentrations translate into two stable uptake fluxes, because the steady states have only two different concentrations for the transporter ($e_1$), which in turn determines the uptake flux via the relation $J = g_1(s_0)e_1$ in equation (6).

### 3.2 Shape and size of the promoter design space

To decide which circuit is the best candidate for an uptake switch, we determined the promoter design spaces and proposed a measure to assess the robustness of each bistable regime. With the simplified model Section 3.1 we obtained analytic conditions for each bistable regime in terms of the promoter dynamic ranges. The conditions are summarised in Fig. 3–4, and the details on how to obtain them are in Appendix A.1 and the Supplementary Material. In particular, the

design spaces for the threshold-independent regimes are:

$$\underline{\text{RR-0 regime}} \quad \beta_1\mu_1 < \mu_{12} < \beta_2\mu_2, \tag{9a}$$
$$\check{\beta}\mu_2 < \mu_{12}. \tag{9b}$$

$$\underline{\text{AA-0 regime}} \quad \beta_1\mu_2 < \mu_{12} < \beta_2\mu_1, \tag{10a}$$
$$\check{\beta}\mu_1 < \mu_{12}. \tag{10b}$$

$$\underline{\text{AR-0 regime}} \quad \beta_1 < \mu_{12} < \beta_2\mu_1\mu_2, \tag{11a}$$
$$\check{\beta}\mu_1\mu_2 < \mu_{12}, \tag{11b}$$

The above conditions, illustrated in Fig. 3, describe all combinations of dynamic ranges the lead to a bistable uptake flux. In all cases, the shape and size of the design space depend on three parameters:

$$\beta_1 = \frac{g_1(s_0)}{g_2(\theta_1)},\ \beta_2 = \frac{g_1(s_0)}{g_2(\theta_2)},\ \check{\beta} = \frac{g_1(s_0)}{g_2^{\text{sat}}}. \tag{12}$$

These parameters reflect how the interplay between enzyme kinetics and gene regulation affects bistability. The $\beta_i$ parameters correspond to the ratio of enzyme turnover rates at a given concentration of extracellular metabolite and transcriptional threshold. They take maximal or minimal values when thresholds are far away from the Michaelis constant of the utilization enzyme ($K_{\text{m}}$). The third parameter, $\check{\beta}$, describes the saturation level of the transport enzyme relative to the maximal utilization rate.

The conditions in (9a)–(11b) assume that the thresholds are ordered as $\theta_1 \leq \theta_2$ (and therefore that $\beta_1 \geq \beta_2$), but the converse conditions for $\theta_1 > \theta_2$ can be obtained by swapping $\beta_1$ and $\beta_2$ in the inequalities. The conditions for bistability in (9a)–(11b) have two parts: a-conditions guarantee two stable steady states for the enzyme concentrations, while b-conditions prevent the accumulation of metabolite in both steady states. The b-conditions arise due to the saturation of the enzyme kinetics: if not satisfied, then the uptake flux will be higher than the saturation rate

of the utilization reaction and cause the metabolite to accumulate in the intracellular space.

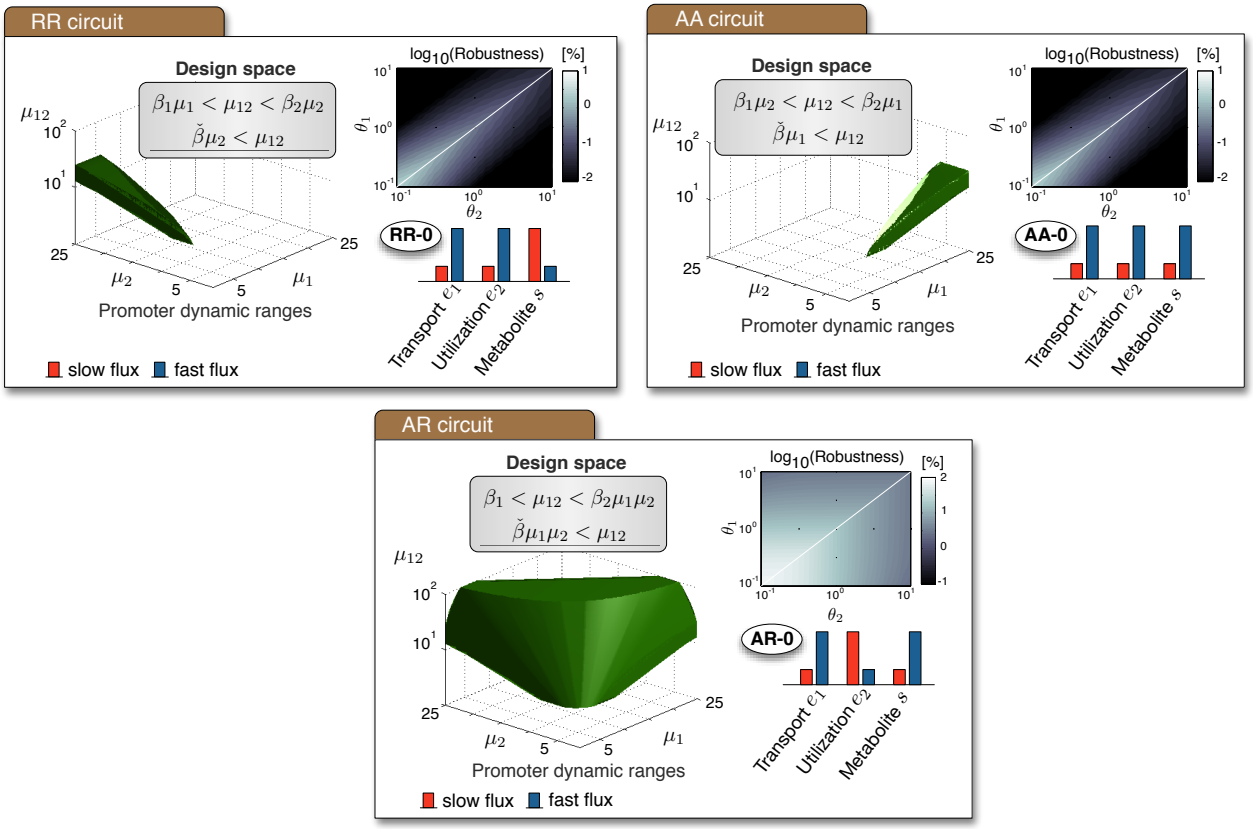


**Figure 3** – Promoter design space for the threshold-independent bistable regimes in Fig. 2. The design spaces can be visualized as 3-dimensional solids in a $(\mu_1, \mu_2, \mu_{12})$ space. The solids correspond to the inequalities in (9a)–(11b) for fixed enzyme kinetics and transcriptional thresholds. The bar plots represent the species concentrations as in Fig. 2. Details on how to find the design spaces analytically are in Appendix A.1 and the Supplementary Material. The size of the design spaces provides a metric for the robustness of each regime. We quantified robustness as the volume of the design space relative to the total volume of the full parameter space for fixed enzyme kinetics and different regulatory thresholds spanning two orders of magnitude. The $(\theta_1, \theta_2)$ values shown are relative to a nominal metabolite concentration $s_0 = 1\mu$M (the white line marks the equal threshold case). Details of the simulations and parameter values can be found in Appendix A.2.

As shown in Fig. 3–4, the shape and size of the design spaces varies significantly across regimes. Bistability in the RR-0 and AA-0 regimes is particularly constrained, as it requires asymmetric designs where one promoter has a much broader dynamic range than the other. The AR-0 regime, in contrast, is much more flexible as it produces bistability for more combinations

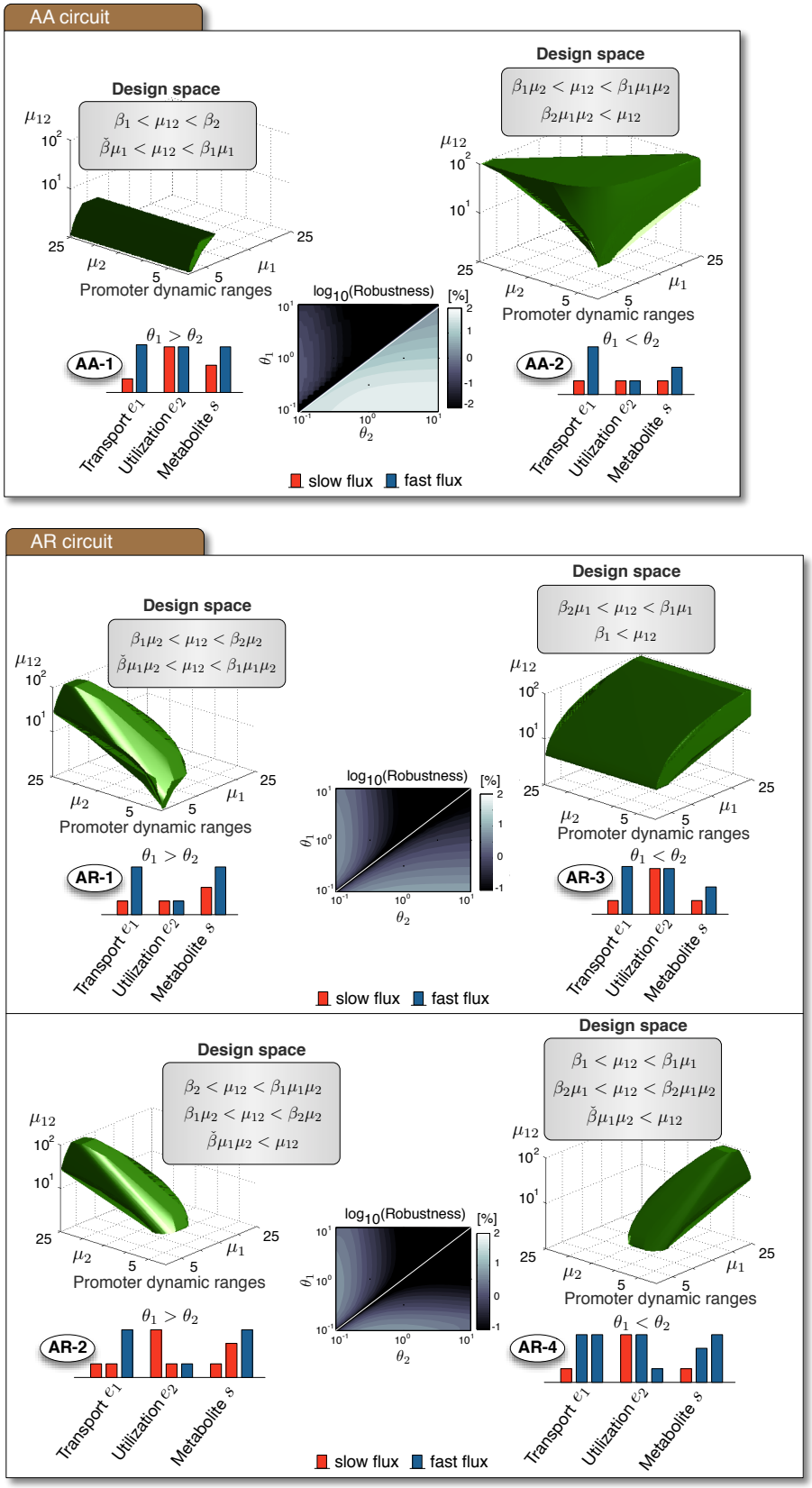


**Figure 4** – Promoter design space for the threshold-dependent bistable regimes in Fig. 2. The design spaces correspond to the shown inequalities for fixed enzyme kinetics and transcriptional thresholds. Details on how to find the design spaces analytically are in Appendix A.1 and the Supplementary Material. The robustness index was computed as in Fig. 3.

of promoter dynamic ranges. We can compare the regimes using the size of their design spaces as a metric for robustness:

$$\text{Robustness} = \frac{\text{Vol}_{\text{bistable}}}{\text{Vol}_{\text{total}}} \times 100, \tag{13}$$

where $\text{Vol}_{\text{bistable}}$ is the volume of the 3-dimensional solid defined by the design space, and $\text{Vol}_{\text{total}}$ is the volume of the full parameter space defined as a cube

$$\begin{aligned} 1 < \mu_1 < \mu_1^{\max}, \\ 1 < \mu_2 < \mu_2^{\max}, \\ \mu_{12}^{\min} < \mu_{12} < \mu_{12}^{\max}. \end{aligned}$$

If we choose the same parameter cube for each circuit, the relative volume provides an effective measure to compare the design spaces. A robust circuit should ideally have a large design space to ensure bistability without a laborious fine-tuning of the promoter's response curve. The design space should also be symmetric with respect to $\mu_1$ and $\mu_2$ to allow for an independent design of both promoters. The most robust bistable circuit would therefore have a 100% relative volume (i.e. all parameter combinations lead to bistability), while fragile designs would have a much smaller volume. Since the design spaces depend strongly on the transcriptional thresholds (through the $\beta_i$ parameters in (12)), we numerically computed the relative volumes of the bistable regimes for different combinations of regulatory thresholds. The results, shown in Fig. 3 and Fig. 4, show that most regimes are fragile, with only two (the AA-2 and AR-0 regimes) standing out with a robustness index above 70%. As observed in Fig. 2, however, the AA-2 regime requires $\theta_1 < \theta_2$ while the AA-0 regime does not impose constraints on the transcriptional thresholds. We therefore conclude that the AR-0 regime is the most robust design for a bistable uptake switch.

The quality of the AR circuit as a bistable switch can be intuitively understood from the interaction diagrams in Fig. 1C. The AR circuit corresponds to two positive feedback loops, where the internalized metabolite increases its own abundance by speeding up its import and slowing down its consumption. Interlinked positive feedback loops are known to improve the bistability properties in a number of natural networks [32, 33, 34] and there is evidence that nature favours bistability through interlinked regulation [2]. In the next sections we carry out a deeper analysis of the AR circuit.

# 4 Further design criteria for the Activation-Repression circuit

## 4.1 Optimization of the promoter design space

Here we use the derived conditions for bistability to learn how to maximize the circuit's design space with the transcriptional thresholds. We focus on the Activation-Repression circuit designed to operate in the robust AR-0 regime, but analyses of the other regimes can be carried out analogously. For this part we further assume that both promoters have equal baseline expression levels, i.e. $E_1^{\text{off}} = E_2^{\text{off}}$ and thus $\mu_{12} = \mu_2$. Substituting $\mu_{12} = \mu_2$ in the conditions in (11a)–(11b), we obtain simplified conditions for bistability

$$\underline{\text{AR-0 regime:}} \quad \begin{aligned} \frac{1}{\beta_2} < \mu_1 < \frac{1}{\check{\beta}}, \\ \mu_2 > \beta_1. \end{aligned} \tag{14}$$

The conditions in (14) describe the design space as an open box in a $(\mu_1, \mu_2)$ parameter space, illustrated in Fig. 5. The effect of the $\beta_i$ parameters in the conditions in (14) suggests a tradeoff between the transcriptional thresholds and the size of the design space (Fig. 5): a low repression threshold $\theta_2$ (i.e. a larger $\beta_2$ parameter) enlarges the design space for the activating promoter ($\mu_1$) and, conversely, a high activation threshold $\theta_1$ enlarges the design space for the repressing promoter ($\mu_2$). Further, we can derive criteria to maximize the design space:

- The upper limit for $\mu_1$ grows if $\check{\beta} \ll 1$. Recalling that $\check{\beta} = g_1(s_0)/g_2^{\text{sat}}$, we conclude that $g_2^{\text{sat}} \gg g_1^{\text{sat}}$ is a sufficient condition for $\check{\beta} \ll 1$ for any concentration of intermediate metabolite. In the case of Michaelis-Menten kinetics, the condition is equivalent to

$$k_{\text{cat}\,2} \gg k_{\text{cat}\,1}. \tag{15}$$

- If $\beta_1 = \beta_2 = 1$ we minimize the lower limits for the dynamic ranges and get a maximal design space

$$\underline{\text{Maximal design space:}} \quad \begin{aligned} 1 < \mu_1 < \frac{1}{\check{\beta}}, \\ \mu_2 > 1. \end{aligned} \tag{16}$$

  Using the definition of the $\beta_i$ parameters ($\beta_i = g_1(s_0)/g_2(\theta_i)$), we can impose the condi-

tion $\beta_i = 1$ to obtain an optimal threshold

$$\theta^\star = g_2^{-1}\left(g_1(s_0)\right), \tag{17}$$

where $g_2^{-1}$ is the inverse function of $g_2$. In the case of Michaelis-Menten kinetics, the inverse is $g_2^{-1}(x) = K_{\mathrm{M}}\, x/(k_{\mathrm{cat}} - x)$. We therefore conclude that if the transcriptional thresholds are designed as

$$\theta_1 \geq \theta^\star \text{ and } \theta_2 \leq \theta^\star, \tag{18}$$

then the AR circuit has a maximal design space for bistability. Note that we state the conditions in (18) as inequalities because, by definition, the dynamic ranges are $\mu_i > 1$ and consequently any combination of thresholds that satisfies (18) leads to the same maximal design space.

The conditions in (15) and (18) provide quantitative criteria for designing an AR circuit with maximal design space for bistability. Condition (15) relaxes the upper limit for the first promoter (dynamic range $\mu_1$), but it is generally difficult to satisfy bacause catalytic enzymes in the same pathway tend to have similar $k_{\mathrm{cat}}$ values. On the other hand, condition (18), illustrated in Fig. 5, loosens the lower limit for the promoter dynamic ranges, and therefore may prove useful in implementations with weak promoters and tuneable regulatory thresholds.

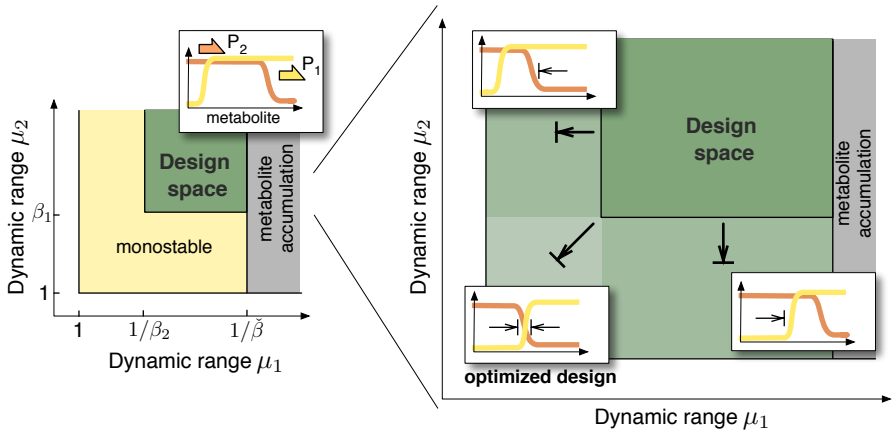


**Figure 5** – Maximization of the design space in the Activation-Repression circuit. The diagrams illustrate the promoter design space for different combinations of transcriptional thresholds, as described by the conditions in (14). The optimal design has regulatory thresholds chosen according to the criteria in (18) taken as equality.

## 4.2 Conditions for hysteresis

So far we have focused on a bistable uptake flux under a fixed amount of extracellular metabolite. A hallmark feature of bistable switches, however, is that they display hysteresis to changes in the input stimulus. As shown in the bifurcation diagram in Fig. 1A, hysteresis causes cells to switch between slow and fast uptake at different metabolite concentrations. This mechanism filters out spurious switching from extracellular fluctuations, and implements a form of memory where the response of a cell to intermediate metabolite concentrations depends on its previous exposure to it. Since equal transcriptional thresholds enlarge the design space (Fig. 3), we assumed a nominal threshold for both promoters, $\theta_1 = \theta_2 = \theta$ and obtained conditions for the AR circuit to display hysteresis:

$$\underline{\text{Hysteresis:}} \qquad \beta_1 < \mu_{12} < \beta_2 \mu_1 \mu_2, \tag{19a}$$

$$\check{\beta}\mu_1\mu_2 < \mu_{12}, \tag{19b}$$

$$\mu_{12} < \hat{\beta}, \tag{19c}$$

$$\beta^{\text{sat}}\mu_1\mu_2 < \mu_{12}, \tag{19d}$$

The above conditions can be obtained by examining the effect of the extracellular metabolite ($s_0$) on the circuit's steady states through changes in the $\beta_i$ parameters (details in Appendix A.1

and the Supplementary Material). The conditions depend on two extra parameters

$$\hat{\beta} = \frac{g_1^{\text{sat}}}{g_2(\theta)}, \quad \beta^{\text{sat}} = \frac{g_1^{\text{sat}}}{g_2^{\text{sat}}}, \tag{20}$$

which correspond to the original $\beta_i$ and $\check{\beta}$ parameters in (12) under saturation of the transport enzyme. The conditions in (19a)–(19b) are the same as the design space in (11), while the conditions in (19c)–(19d) add further constraints to the design space. Condition (19c) guarantees that uptake can be bidirectionally switched, i.e. from slow to fast and *vice versa* (if not satisfied, the circuit can only be switched off). Condition (19d) ensures that the metabolite steady state $\bar{s}$ exists for all concentrations of extracellular metabolite. Note that the condition (19d) becomes less tight under the kinetic condition in (15).

# 5 Activation-Repression circuit with graded promoters

## 5.1 Validation of the design criteria

In the previous sections we obtained design criteria for the AR circuit based on a coarse approximation for promoter activity. The approximation assumes that promoters behave in an on-off fashion, i.e. having either a maximal or baseline activity without intermediate levels of expression. In practical implementations, promoter sensitivities are severely constrained and therefore it is unclear whether the derived design criteria are useful when using realistic promoters with graded, low-sensitivity, response curves.

To test the utility of the AR circuit in a more realistic model, we ran extensive simulations of the circuit with sigmoidal models for promoter response curves [35]. We modelled the promoter response curves as Hill functions

$$\sigma_1(s) = \frac{s^h}{\theta^h + s^h}, \quad \sigma_2(s) = \frac{\theta^h}{\theta^h + s^h} \tag{21}$$

where $\theta$ is the regulatory threshold and $h$ is the promoter sensitivity (Hill coefficient). We computed the parameter regions for bistability in the continuous model (1)–(2) with low, intermediate and high promoter sensitivities. The results in Fig. 6A suggest that although the design spaces for the continuous model are smaller than those predicted by our approximation, they preserve the predicted qualitative properties (compare Figures 5 and 6A). We can distinguish

among designs that are monostable, bistable, or that do not have a steady state. Optimization of the regulatory threshold, i.e. according to the criterion in (18), effectively enlarges the design space in the continuous model, even in the case of low-sensitivity promoters ($h = 2$). These results thus suggest that the derived design criteria can guide the design in more realistic models for promoter activities.

In Fig. 6B we plot the domains of attraction for each steady state in particular instances of AR circuits with low-sensitivity promoters. The results suggest that basins of attraction can depend strongly on the transcriptional thresholds and, in particular, threshold-optimization can also help to equalize the domains of attraction and prevent a bias towards one uptake flux more than the other. The bifurcation diagrams in Fig. 6C indicate that the AR circuit effectively functions as a bidirectional switch with hysteresis, toggling between low/high states for enzyme expression.

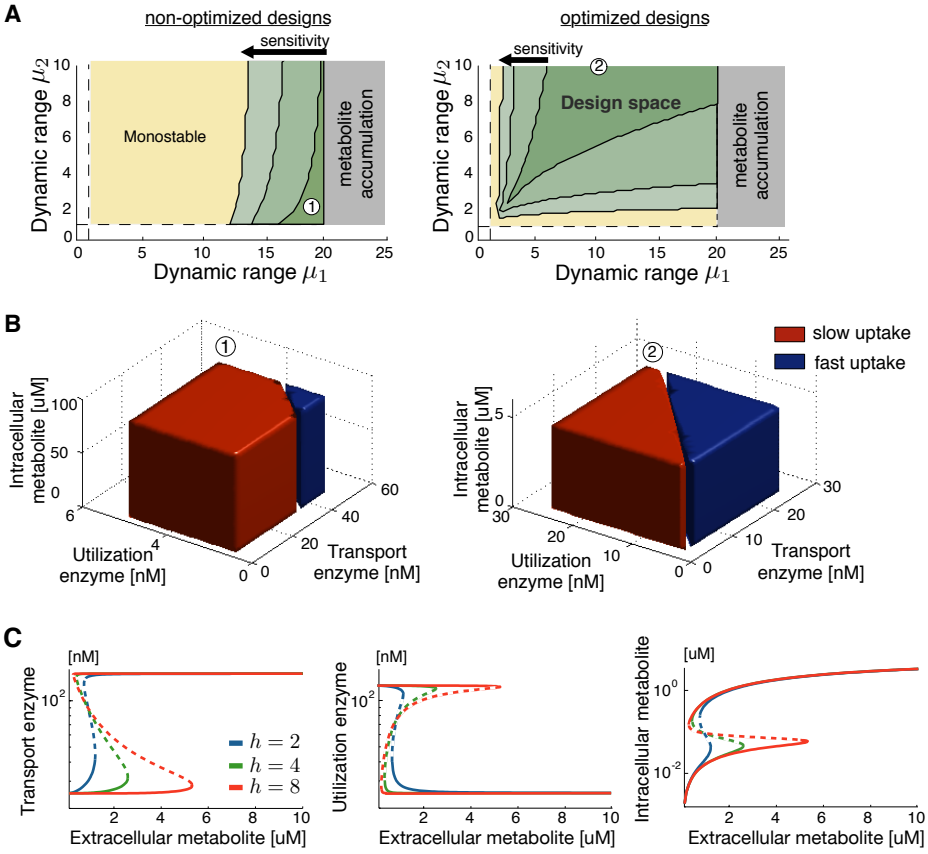


**Figure 6** – Bistability in the Activation-Repression circuit. (**A**) Regions for bistability in non-optimized and optimized designs for a continuous model of the AR circuit (cf. Fig. 5). In the non-optimized designs the regulatory threshold was chosen as $\theta = s_0$ for an extracellular metabolite concentration $s_0 = 4.7\mu$M; in the optimized designs the threshold was chosen to maximize the region for bistability according to the criterion in (18) taken as equality; promoter sensitivities are $h = \{2, 4, 8\}$. (**B**) Domains of attraction of two specific designs with low-sensitivity promoters ($h = 2$) and promoter dynamic ranges $(\mu_1, \mu_2) = (19, 2)$ and $(\mu_1, \mu_2) = (10, 10)$, marked as ① and ② in panel **A**. (**C**) Bifurcation diagrams of the enzyme concentrations and internalized metabolite as a function of the extracellular concentration; solid (dashed) lines indicate the stable (unstable) steady states. The design is optimized for a nominal concentration $s_0 = 1\mu$M according to (18) taken as equality, and promoter dynamic ranges $(\mu_1, \mu_2) = (6, 5)$. The baseline enzyme expression levels were fixed to $E_1^{\text{off}} = E_2^{\text{off}} = 2.5$nM in panels **A**–**B**, and $E_1^{\text{off}} = E_2^{\text{off}} = 25$nM in panel **C**. Details of the simulations and parameter values can be found in Appendix A.2.

## 5.2 Emergence of bimodal phenotypes across cell populations

Our results describe conditions under which single cells display a bistable uptake when exposed to the extracellular metabolite. At a population level, however, each individual cell will switch to slow or fast uptake depending on its intracellular state before exposure to the metabolite. Due to numerous factors that affect the cellular composition, cell populations can exhibit a large cell-to-cell variability. In the case of synthetic gene circuits, variability can arise from e.g. fluctuations in plasmid copy numbers, variability in transcriptional and translational resources (RNA polymerases, sigma factors and ribosomes), mutations in the promoter sequences, and the stochastic fluctuations inherent to gene expression [36].

We ran population-wide simulations of the AR circuit to test how it would perform in bacterial cultures with significant cell-to-cell variability. The domains of attraction in Fig. 6B suggest that single cells switch to a slow or fast uptake depending only on the abundance of enzymes and not the intracellular metabolite. We therefore focused on how variability in enzyme levels propagates to the flux phenotypes produced by the uptake switch [37, 38]. We modelled variability in enzyme expression through deterministic simulations for many cells in a culture with randomized promoter dynamic ranges. The results, shown in Fig. 7, indicate that the proposed AR circuit can effectively toggle the uptake flux in a population. The resulting population-wide histograms show the hysteretic response of the uptake switch, with individual cells switching to a slow or fast uptake depending on their previous exposure to extracellular metabolite. As predicted by the bifurcation diagrams in Fig. 6C, the range for hysteresis grows with more sensitive promoters and further, we found that the high flux state has a narrow distribution that is largely insensitive to the Hill coefficient. This indicates that the AR circuit tightly controls the uptake flux across a population even for low sensitivity promoters. As a consequence of cell-to-cell variability, individual cells switch at different extracellular concentrations of the metabolite, leading to the observed bimodal phenotypes when the metabolite is close to the switching threshold.

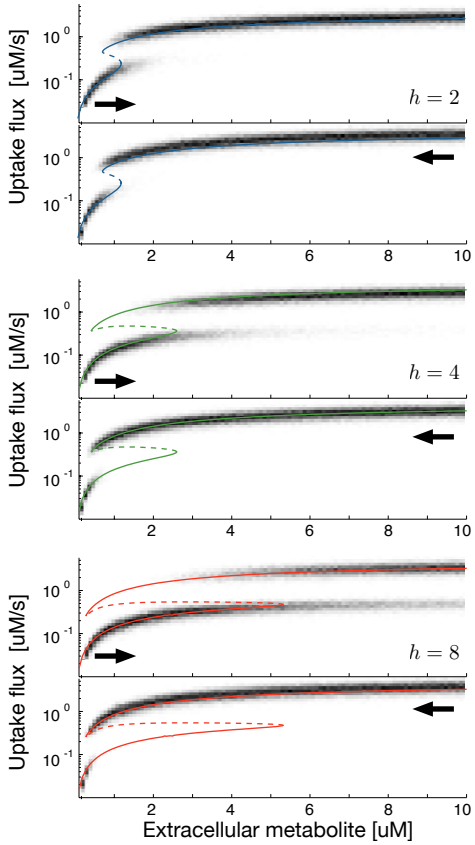


**Figure 7** – Hysteresis and bimodal phenotypes in the Activation-Repression circuit. Response of a cell population with variability in the enzyme expression levels. The heat maps are histograms of the population-wide distributions of the uptake flux for increasing or decreasing levels of extracellular metabolite. Cell populations were initialized at low (top panels) or high (bottom panels) uptake fluxes. The grayscale represents the number of cells with a given uptake flux. The histograms were obtained from a population with 500 cells with enzyme expression levels ($E_i^{\text{off}}$ and $E_i^{\text{on}}$) sampled from Gamma distributions [39] with means corresponding to the designs in Fig. 6C and a coefficient of variation of 20%, representative of measured genome-wide fluctuations in protein abundance [40]. The circuit is optimized for a nominal metabolite concentration $s_0 = 1\mu$M according to the criterion in (18) taken as equality. The histograms are overlaid with the flux bifurcation diagrams computed from Fig. 6C. Details of the simulations and parameter values can be found in Appendix A.2.

# 6 Discussion

In this paper we proposed a bistable switch to control the rate at which cells take up a metabolite from the environment. The switch couples enzyme activity with a two-promoter gene network

under feedback regulation. We examined mathematical models for four candidate networks and obtained the design spaces for promoter dynamic ranges that produce a bistable uptake system. Using the size of the promoter design space as a proxy for robustness, we singled out one network, an Activation-Repression circuit (AR in Fig. 1C), that is significantly more robust than the others and is the best candidate for an uptake switch.

The proposed Activation-Repression circuit effectively toggles between slow and fast uptake depending on the abundance of the extracellular metabolite. The shape of its design space suggests that both promoters can be tuned independently and we found criteria to maximise the design space by tuning the transcriptional thresholds. The large design space also indicates that the switch is robust to variability in promoter strengths and thus requires little fine-tuning of promoter response curves. Population-wide simulations show the emergence of bimodal phenotypes due to cell-to-cell variability and hysteresis. The circuit thus works as a memory device where individual cells lock into slow or fast uptake depending on their previous exposure to the extracellular metabolite, while protecting them from spurious switching caused by stochastic environmental fluctuations.

A key element in the proposed switch is the use of feedback regulation of enzyme expression levels. This strategy was inspired by the regulation of the lactose operon in *E. coli* [19] and the galactose pathway in *S. cerevisiae* [14], two well known uptake systems where bistability emerges from the interplay between metabolism and gene regulation. In the lactose operon, bistability emerges from a regulatory architecture similar to the Activation-Activation circuit studied here, but our results indicate it is not as robust as the Activation-Repression circuit because it requires more careful fine-tuning of the design parameters. Natural systems may achieve such fine-tuning through evolution, but this is extremely laborious in engineered systems. In the galactose pathway, on the other hand, bistability emerges from a more complex gene regulatory network with multiple components and interactions that are difficult to tease apart. Other bacterial systems that display switching metabolic phenotypes, e.g. the carbon catabolite repression system [41], the glycolytic-gluconeogenic switch [42] and the central carbon metabolism [43], rely on even more intricate regulation and are too complex to be used as templates for design. Although other strategies to produce bistability may exist, either using different genetic circuits or regulatory mechanisms, the proposed Activation-Repression circuit is a simple architecture for a robust uptake switch, and thus a promising backbone for future implementations.

The uptake switch provides an interface to control metabolic activity from the extracellular space. This could be useful, for example, in metabolic engineering applications that need to reg-

ulate production with extracellular inducers or to trigger pathways only when substrates reach an activation threshold. The hysteretic response of the switch can help to control production in face of substrate variability or heterogeneous bioreactor conditions. Another promising application for a bistable uptake switch is the control and coordination of metabolism in microbial consortia. Although most synthetic cell-to-cell communication systems rely on mechanisms drawn from quorum sensing or hormone signalling, recent studies have also explored the use of metabolic signals to coordinate pathways distributed among different strains [44]. The field is in its early days, but it is becoming increasingly clear that metabolites may not only provide a new channel for synthetic communication between cells [12], but also that consortia can outperform single-strain cultures [13]. A plausible scenario for this is, for example, to split a large synthetic pathway among different strains and thus alleviate the genetic burden caused by expression of multiple heterologous proteins in a single strain [45]. The general principle is to have a "sender" strain that secretes a metabolite which is then taken up by a "receiver" strain. If the exchanged metabolite is a precursor for a target product in the receiver strain, an uptake switch can serve as a mechanism to lock receivers in a high uptake flux and, through hysteresis, insulate them from extracellular fluctuations in the transmitted signal. Another possibility is to use the uptake switch in receiver cells to diversify their phenotypes. Upon command from sender cells, receivers can split into slow- and fast-feeders, opening up the possibility to use bet-hedging to control metabolic activity upon changes in growth conditions, a well-known survival strategy used by microbes [15]. Such synthetic systems could also be used to study the evolution of social interactions in microbes. A number of studies have successfully used synthetic gene circuits to uncover how strains evolve their phenotypes in different conditions, e.g. under competition for shared carbon sources or cooperation through exchange of nutrients and signalling molecules [16, 46, 47]. These diverse applications suggest that bistable uptake switches will become increasingly relevant as efforts to engineer synthetic consortia intensify in the future.

Asserting whether a biochemical network is bistable is a challenging mathematical and computational problem. For specific classes of models, a number of approaches have addressed bistability by e.g. exploiting the structure of the model's Jacobian [28, 48] or using notions from Chemical Reaction Network Theory [49] (see [50, Table 3] for a list of existing approaches). Finding parameter regions for bistability is even harder and, although promising approaches exist for specific model types [51], for more general models the problem remains largely unsolved and we do not have effective methods other than numerical exploration of the parameter space.

We overcame the above limitations with an analysis technique that combines a piecewise

affine model for gene expression, a kinetic model for metabolic reactions, and a separation of timescales between both [21]. This strategy proved useful to single out networks that display bistability and to identify the parameter design spaces analytically. A salient conclusion of our analysis is that the uptake systems display a diverse range of bistable regimes. The Activation-Repression circuit, in particular, displays five qualitatively different bistable regimes depending on the promoter dynamic ranges and their transcriptional thresholds. Our approach also offers a number of other advantages: it requires minimal assumptions on the enzyme kinetics, it accounts for the four regulatory circuits simultaneously without separate *ad hoc* analyses, and it reveals the underlying geometry of the design space for bistability in terms of experimentally accessible parameters. The latter uncovers how the interplay between promoter design and enzyme kinetics affects the shape and size of the design space, giving a first idea of which design parameters are most relevant to achieve a prescribed phenotype.

We point out that because our analysis relies on a coarse on-off approximation of promoters, its predictions are not guaranteed to hold in more realistic models for promoter activity. Our simulation results show, however, that the derived design criteria can effectively guide circuit design in models with standard sigmoidal descriptions of promoter response curves, even in the case of low Hill numbers, and that the derived design spaces provide an excellent starting point to search for bistability.

In this work we focused on the promoter dynamic ranges as the main tuneable parameters of the circuits. Although new technologies in DNA engineering are ever expanding the number of tuneable "knobs" in synthetic circuits [52, 53], promoter dynamic ranges are particularly flexible in that they can be altered with many techniques, e.g. by random mutagenesis [26], by manipulation of polymerase binding sites [54], or by the addition of sequence repeats [55]. In its current form, our model analysis can also be used to study the effect of tuneable protein half-lives [56], the strength of ribosomal binding sites [27], and in general, other genetic modifications that can be modelled as a linear scaling of protein expression rates. Other tuning strategies, e.g. affinity of transcription factors or post translational modifications, however, cannot be directly included in our analysis and require a more mechanistic model for gene expression beyond the lumped model used here.

Our main goal in this paper has been to investigate the mathematical design of an uptake switch. We sought to draw analytic links between bistability and design parameters, for which we studied a tractable model that retains the typical nonlinearities encountered in enzyme kinetics and gene regulation. The costs of this analytic treatment were a number of model sim-

plifications that should be addressed in future molecular implementations of the switch. First, the model should include the mechanistic details for gene regulation. By including the detailed interactions between the internalised metabolite and enzyme expression, the model will predict the effect of the particular strategy used to tune the circuit function. Second, the model should be tailored to the specific metabolite and enzymes employed, including features such as reversible transport or regulatory mechanisms of kinetic activity. Third, the model should account for the interactions between the uptake switch and its host. These can significantly degrade the function of genetic circuits [57] and recent progress in models for bacterial growth allow to systematically incorporate host-circuit interactions into the circuit design [58]. This will be particularly relevant for switches designed to take up carbon sources or essential nutrients, as these will likely interfere with central metabolic functions of the host and trigger some of its native regulatory mechanisms [59].

The molecular implementation of the proposed switch remains a challenge because of the lack of mechanisms to sense intracellular metabolites and control gene expression. Natural systems have evolved a number of mechanisms to sense intracellular metabolites, see e.g. the comprehensive discussions in [59, 60], but in general it is not easy to make them respond to metabolites they have not evolved to sense [25]. The lack of metabolite sensors is the most important bottleneck in dynamic metabolic engineering [24] and limits all current efforts to engineer synthetic gene circuits for metabolism. In our study we have assumed that the intracellular metabolite controls enzyme expression by direct activation or repression of the promoters, but in implementations the regulation will be mediated by a specific molecular mechanism, e.g. natural metabolite-responsive transcription factors [8] or hybrid promoter-regulator systems [61]. Although currently there are no modular mechanisms to sense intracellular metabolites, recent progress in the field has led to e.g. novel sensors [25] and the implementation of a Repression-Activation circuit in *E. coli* [10], bringing us increasingly close to building complex genetic-metabolic circuitry. This makes the role of mathematical design ever more important, as it is a powerful tool to discover useful circuit architectures that could be built once metabolite sensors are available.

## Acknowledgments

We thank Jordan Ang, John Heap, Andrea Weiße and Fuzhong Zhang for helpful suggestions.

## Funding Statement

Diego Oyarzún was supported in part by Imperial College London through a Junior Research Fellowship and the Human Frontier Science Program through a Young Investigator Grant (RGY0076/2015). Madalena Chaves was supported in part by projects GeMCo (ANR-2010-BLAN-0201-01) and Labex Signalife (ANR-11-LABX-0028-01).

## Competing interests

We have no competing interests.

# A Appendix

### A.1 Analytic results

**Identification of bistable regimes and parameter spaces for bistability** The details on how to identify each bistable regime in Fig. 2, together with their conditions for bistability (the design spaces in Fig. 3–4), can be found in the Supplementary Material. The general idea is to first approximate the promoter response curves in the model (1)–(2) by step functions:

$$\frac{\mathrm{d}s}{\mathrm{d}t} = g_1(s_0)e_1 - g_2(s)e_2, \tag{A1}$$

$$\begin{aligned}\frac{\mathrm{d}e_1}{\mathrm{d}t} &= \kappa_1^0 + \kappa_1^1\bar{\sigma}_1(s) - \gamma_1 e_1,\\ \frac{\mathrm{d}e_2}{\mathrm{d}t} &= \kappa_2^0 + \kappa_2^1\bar{\sigma}_2(s) - \gamma_2 e_2,\end{aligned} \tag{A2}$$

where $\bar{\sigma}_i$ are the step functions in (8). Using the separation of timescales, we reduce the model assuming the metabolite to be in quasi steady state with respect to the evolution of enzyme concentrations. Details on the technical conditions for the separation of timescales can be found in [62]. We take $\mathrm{d}s/\mathrm{d}t \approx 0$ in equation (A1) to get an algebraic equation for the metabolite concentration

$$g_2(s) = g_1(s_0)\frac{e_1}{e_2}. \tag{A3}$$

The key observation is that, since $g_2(s)$ is an increasing function of $s$, the condition $s < \theta_i$ implies that $g_2(s) < g_2(\theta_i)$, which after substituting in (A3) leads to the equivalences:

$$s < \theta_i \iff e_2/e_1 > \beta_i, \quad s > \theta_i \iff e_2/e_1 < \beta_i, \tag{A4}$$

where $\beta_i = g_1(s_0)/g_2(\theta_i)$ are the parameters that appear in all the conditions for bistability (Fig. 3–4). We can then get a reduced model in the form of a 2-dimensional discontinuous differential equation

$$\frac{\mathrm{d}e}{\mathrm{d}t} = \Gamma\left(\phi - e\right), \tag{A5}$$

where $e = [e_1, e_2]$ is the vector of enzyme concentrations and the matrix $\Gamma = \mathrm{diag}\{\gamma_1, \gamma_2\}$ contains the degradation rates. The vector $\phi$ is piecewise constant and is formed by different combinations of baseline ($E_i^{\mathrm{off}}$) and maximal ($E_i^{\mathrm{on}}$) enzyme expression levels, depending on whether $e_1/e_2 > \beta_i$ or $e_1/e_2 < \beta_i$. The model in (A5) is a piecewise affine differential equation defined in conic domains (because conditions such as $e_1/e_2 > \beta_i$ describe a cone in an $(e_1, e_2)$ plane). We can then identify its bistable regimes and the conditions for bistability by examining the geometry of the partitioned state space. The conditions for bistability arise naturally in terms of $E_i^{\mathrm{off}}$ and $E_i^{\mathrm{on}}$ concentrations, but we can convert them to conditions on the promoter dynamic ranges with the following equivalences (recall the definitions in (3)–(5)):

$$\begin{aligned} E_1^{\mathrm{off}}/E_2^{\mathrm{off}} = \mu_2/\mu_{12}, \quad E_1^{\mathrm{on}}/E_2^{\mathrm{on}} = \mu_1/\mu_{12}, \\ E_1^{\mathrm{on}}/E_2^{\mathrm{off}} = \mu_1\mu_2/\mu_{12}, \quad E_2^{\mathrm{on}}/E_1^{\mathrm{off}} = \mu_{12}. \end{aligned} \tag{A6}$$

**Conditions for hysteresis in the Activation-Repression circuit** We can obtain the conditions for hysteresis in the AR circuit (the inequalities in (19a)–(19d)) by examining the model's bistability with the parameters $\beta_i = g_1(s_0)/g_2(\theta_i)$ regarded as functions of the extracellular metabolite ($s_0$). The key idea is to ensure that: for low $s_0$ concentrations the model is monostable with a slow uptake flux, for intermediate $s_0$ concentrations the model is bistable, and for high $s_0$ concentrations the model is monostable with a fast uptake flux. These three conditions guarantee that the piecewise model has two saddle-node-like bifurcations and thus displays hysteresis. Further details can be found in the Supplementary Material.

## A.2 Model simulations

Simulations were done in Matlab with enzyme kinetic parameters $k_{\text{cat}\,1} = 32\text{s}^{-1}$, $k_{\text{cat}\,2} = 320\text{s}^{-1}$, $K_{\text{M}\,1} = K_{\text{M}\,2} = 4.7\mu\text{M}$, and enzyme degradation rate constants $\gamma_1 = \gamma_2 = 2 \times 10^{-4}\text{s}$, corresponding to a half-life $\sim$1h.

**Size of promoter design spaces.** To compute the volumes of the solids in Fig. 3 and Fig. 4, we computed the convex hull of points satisfying the inequalities that define each design space. The $\mu_1$ and $\mu_2$ axis contains 50 linearly spaced points each, with $\mu_1^{\text{max}} = \mu_2^{\text{max}} = 25$. The $\mu_{12}$ axis contains 50 log-spaced points with $(\mu_{12}^{\text{min}}, \mu_{12}^{\text{max}}) = (10^{-2}, 10^2)$.

**Simulations of the continuous model.** We determined the parameter regions for bistability (Fig. 6A) from long simulations of the model in (1)–(2) for $10^4$ pairs of promoter dynamic ranges $(\mu_1, \mu_2)$ and $\mu_{12} = \mu_2$ sampled from a regular grid with increasing promoter sensitivities ($h_i = \{2, 4, 8\}$ for $i = 1, 2$). We ran two simulations for each $(\mu_1, \mu_2)$ pair, initialized at the two stable steady states predicted by the piecewise affine model. We discriminated between monostability and bistability using the euclidean distance between the final time points of each simulation. We determined the regions for metabolite accumulation by checking the condition $g_2(\bar{s}) < g_2^{\text{sat}}$ at the final time points (in which case the steady state equation in (7) does not have a solution).

We computed the domains of attraction in Fig. 6B from long simulations of (1)–(2) for $8 \times 10^3$ initial conditions sampled from a uniform grid. The bifurcation diagrams in Fig. 6C were computed with the MatCont package for Matlab [63].

**Population-wide simulations.** We computed the the histograms in Fig. 7 from simulations of the deterministic model (1)–(2) with randomized parameters. The top/bottom panels in Fig. 7 are simulations of cells initialized at a low/high uptake fluxes in steady state, and each simulation was ran for 100 increasing/decreasing concentrations of extracellular metabolite in the range $[0.1, 10]\mu\text{M}$. For a each metabolite concentration $s_0$, we sampled the baseline and maximal enzyme concentrations ($E_i^{\text{off}}$ and $E_i^{\text{on}}$ for $i = 1, 2$) from Gamma distributions with means $\langle E_1^{\text{off}} \rangle = \langle E_2^{\text{off}} \rangle = 25\text{nM}$, $\langle E_1^{\text{on}} \rangle = 150\text{nM}$, and $\langle E_2^{\text{on}} \rangle = 125\text{nM}$, which correspond to dynamic ranges $(\mu_1, \mu_2) = (6, 5)$; these are the same parameters as in the bifurcation diagrams in Fig. 6C. We used a coefficient of variation of 20%, representative of measured fluctuations

in protein abundance reported in the literature [40]. The gene expression parameters were then computed as $\kappa_i^0 = \gamma_i E_i^{\text{off}}$ and $\kappa_i^1 = \gamma_i \left(E_i^{\text{on}} - E_i^{\text{off}}\right)$. The histograms were obtained from simulations of 500 cells for each concentration $s_0$; we discarded and resampled all samples that led to metabolite accumulation by checking the condition $g_2(\bar{s}) < g_2^{\text{sat}}$ at the final time points of the simulation.

# References


[1] J. J. Tyson, K. C. Chen, and B. Novak, "Sniffers, buzzers, toggles and blinkers: dynamics of regulatory and signaling pathways in the cell," *Current Opinion in Cell Biology*, vol. 15, no. 2, pp. 221–231, Apr. 2003.

[2] O. Brandman, J. E. Ferrell, R. Li, and T. Meyer, "Interlinked fast and slow positive feedback loops drive reliable cell decisions." *Science*, vol. 310, no. 5747, pp. 496–8, Oct. 2005.

[3] T. S. Gardner, C. R. Cantor, and J. J. Collins, "Construction of a genetic toggle switch in Escherichia coli," *Nature*, vol. 403, no. 6767, pp. 339–342, Jan. 2000.

[4] M. R. Atkinson, M. A. Savageau, J. T. Myers, and A. J. Ninfa, "Development of Genetic Circuitry Exhibiting Toggle Switch or Oscillatory Behavior in Escherichia coli," *Cell*, vol. 113, no. 5, pp. 597–607, May 2003.

[5] B. P. Kramer and M. Fussenegger, "Hysteresis in a synthetic mammalian gene network." *Proceedings of the National Academy of Sciences of the United States of America*, vol. 102, no. 27, pp. 9517–22, July 2005.

[6] D. Chen and A. P. Arkin, "Sequestration-based bistability enables tuning of the switching boundaries and design of a latch." *Molecular systems biology*, vol. 8, no. 1, p. 620, Jan. 2012.

[7] W. R. Farmer and J. C. Liao, "Improving lycopene production in *Escherichia coli* by engineering metabolic control," *Nature Biotechnology*, vol. 18, no. 5, pp. 533–537, May 2000.

[8] F. Zhang, J. M. Carothers, and J. D. Keasling, "Design of a dynamic sensor-regulator system for production of chemicals and fuels derived from fatty acids," *Nature Biotechnology*, vol. 30, pp. 354–359, Mar. 2012.

[9] D. A. Oyarzún and G.-B. V. Stan, "Synthetic gene circuits for metabolic control: design trade-offs and constraints," *Journal of The Royal Society Interface*, vol. 10, no. 78, p. 20120671, 2013.

[10] P. Xu, L. Li, F. Zhang, G. Stephanopoulos, and M. Koffas, "Improving fatty acids production by engineering dynamic pathway regulation and metabolic control," *Proceedings of the National Academy of Sciences*, vol. 111, no. 31, pp. 11 299–11 304, aug 2014.

[11] E. Fung, W. W. Wong, J. K. Suen, T. Bulter, S.-g. Lee, and J. C. Liao, "A synthetic gene-metabolic oscillator," *Nature*, vol. 435, no. 7038, pp. 118–122, May 2005.

[12] R. Silva-Rocha and V. de Lorenzo, "Engineering multicellular logic in bacteria with metabolic wires." *ACS synthetic biology*, vol. 3, no. 4, pp. 204–9, Apr. 2014.

[13] K. Brenner, L. You, and F. H. Arnold, "Engineering microbial consortia: a new frontier in synthetic biology." *Trends in biotechnology*, vol. 26, no. 9, pp. 483–9, Sept. 2008.

[14] M. Acar, A. Becskei, and A. van Oudenaarden, "Enhancement of cellular memory by reducing stochastic transitions." *Nature*, vol. 435, no. 7039, pp. 228–32, May 2005.

[15] A. Solopova, J. van Gestel, F. J. Weissing, H. Bachmann, B. Teusink, J. Kok, and O. P. Kuipers, "Bet-hedging during bacterial diauxic shift." *Proceedings of the National Academy of Sciences of the United States of America*, vol. 111, no. 20, pp. 7427–32, May 2014.

[16] A. Kashiwagi, I. Urabe, K. Kaneko, and T. Yomo, "Adaptive response of a gene network to environmental changes by fitness-induced attractor selection." *PloS one*, vol. 1, no. 1, p. e49, Jan. 2006.

[17] A. Goldbeter and D. E. Koshland, "An amplified sensitivity arising from covalent modification in biological systems." *Proceedings of the National Academy of Sciences*, vol. 78, no. 11, pp. 6840–6844, Nov. 1981.

[18] A. Ciliberto, F. Capuani, and J. J. Tyson, "Modeling networks of coupled enzymatic reactions using the total quasi-steady state approximation." *PLoS computational biology*, vol. 3, no. 3, p. e45, Mar. 2007.

[19] E. Ozbudak, M. Thattai, H. Lim, B. Shraiman, and A. van Oudenaarden, "Multistability in the lactose utilization network of *Escherichia coli*," *Nature*, vol. 427, pp. 737–740, 2004.

[20] C. Cosentino, L. Salerno, A. Passanti, A. Merola, D. G. Bates, and F. Amato, "Structural bistability of the GAL regulatory network and characterization of its domains of attraction." *Journal of computational biology : a journal of computational molecular cell biology*, vol. 19, no. 2, pp. 148–62, Feb. 2012.

[21] D. A. Oyarzún, M. Chaves, and M. Hoff-Hoffmeyer-Zlotnik, "Multistability and oscillations in genetic control of metabolism." *Journal of Theoretical Biology*, vol. 295, pp. 139–153, 2012.

[22] R. Casey, H. de Jong, and J.-L. Gouzé, "Piecewise-linear models of genetic regulatory networks: equilibria and their stability," *Journal of Mathematical Biology*, vol. 52, pp. 27–56, 2006.

[23] A. Dayarian, M. Chaves, E. D. Sontag, and A. M. Sengupta, "Shape, size, and robustness: feasible regions in the parameter space of biochemical networks." *PLoS computational biology*, vol. 5, no. 1, p. e1000256, Jan. 2009.

[24] I. M. Brockman and K. L. J. Prather, "Dynamic metabolic engineering: New strategies for developing responsive cell factories," *Biotechnology Journal*, vol. 10, no. 9, pp. 1360–1369, sep 2015.

[25] D. Liu, T. Evans, and F. Zhang, "Applications and advances of metabolite biosensors for metabolic engineering," *Metabolic Engineering*, vol. 31, pp. 35–43, sep 2015.

[26] H. Alper, C. Fischer, E. Nevoigt, and G. Stephanopoulos, "Tuning genetic control through promoter engineering." *Proceedings of the National Academy of Sciences of the United States of America*, vol. 102, no. 36, pp. 12 678–83, Sept. 2005.

[27] H. M. Salis, E. A. Mirsky, and C. A. Voigt, "Automated design of synthetic ribosome binding sites to control protein expression." *Nature biotechnology*, vol. 27, no. 10, pp. 946–50, Oct. 2009.

[28] M. Kaufman, C. Soulé, and R. Thomas, "A new necessary condition on interaction graphs for multistationarity," *Journal of Theoretical Biology*, vol. 248, no. 4, pp. 675–685, oct 2007.

[29] H. de Jong, J.-L. Gouzé, C. Hernandez, M. Page, T. Sari, and J. Geiselmann, "Qualitative simulation of genetic regulatory networks using piecewise-linear models," *Bulletin of Mathematical Biology*, vol. 2, pp. 301–340, 2004.

[30] D. Ropers, V. Baldazzi, and H. de Jong, "Model reduction using piecewise-linear approximations preserves dynamic properties of the carbon starvation response in escherichia coli." *IEEE/ACM Transactions on Computational Biology and Bioinformatics*, vol. 8, no. 1, pp. 166–81, Jan. 2011.

[31] U. Alon, *An introduction to systems biology: design principles of biological circuits*. Chapman & Hall/CRC, 2006.

[32] K. Sriram, S. Soliman, and F. Fages, "Dynamics of the interlocked positive feedback loops explaining the robust epigenetic switching in Candida albicans." *Journal of theoretical biology*, vol. 258, no. 1, pp. 71–88, May 2009.

[33] M. R. Domingo-Sananes and B. Novak, "Different effects of redundant feedback loops on a bistable switch." *Chaos*, vol. 20, no. 4, p. 045120, Dec. 2010.

[34] A. Tiwari and O. A. Igoshin, "Coupling between feedback loops in autoregulatory networks affects bistability range, open-loop gain and switching times." *Physical biology*, vol. 9, no. 5, p. 055003, Oct. 2012.

[35] G. Yagil and E. Yagil, "On the relation between effector concentration and the rate of induced enzyme synthesis." *Biophysical journal*, vol. 11, no. 1, pp. 11–27, Jan. 1971.

[36] A. Raj and A. van Oudenaarden, "Single-molecule approaches to stochastic gene expression." *Annual review of biophysics*, vol. 38, pp. 255–70, Jan. 2009.

[37] P. Labhsetwar, J. A. Cole, E. Roberts, N. D. Price, and Z. A. Luthey-Schulten, "Heterogeneity in protein expression induces metabolic variability in a modeled Escherichia coli population." *Proceedings of the National Academy of Sciences of the United States of America*, vol. 110, no. 34, pp. 14 006–11, Aug. 2013.

[38] D. A. Oyarzún, J.-B. Lugagne, and G.-B. Stan, "Noise propagation in synthetic gene circuits for metabolic control." *ACS Synthetic Biology*, vol. 4, no. 2, pp. 116–125, Apr. 2015.

[39] V. Shahrezaei and P. S. Swain, "Analytical distributions for stochastic gene expression." *Proceedings of the National Academy of Sciences of the United States of America*, vol. 105, no. 45, pp. 17 256–61, Nov. 2008.

[40] Y. Taniguchi, P. J. Choi, G.-W. Li, H. Chen, M. Babu, J. Hearn, A. Emili, and X. S. Xie, "Quantifying E. coli proteome and transcriptome with single-molecule sensitivity in single cells." *Science*, vol. 329, no. 5991, pp. 533–538, July 2010.

[41] A. Kremling, J. Geiselmann, D. Ropers, and H. de Jong, "Understanding carbon catabolite repression in Escherichia coli using quantitative models." *Trends in microbiology*, vol. 23, no. 2, pp. 99–109, Feb. 2015.

[42] O. Kotte, B. Volkmer, J. L. Radzikowski, and M. Heinemann, "Phenotypic bistability in Escherichia coli's central carbon metabolism." *Molecular systems biology*, vol. 10, no. 7, p. 736, Jan. 2014.

[43] J. H. van Heerden, M. T. Wortel, F. J. Bruggeman, J. J. Heijnen, Y. J. M. Bollen, R. Planqué, J. Hulshof, T. G. O'Toole, S. A. Wahl, and B. Teusink, "Lost in transition: start-up of glycolysis yields subpopulations of nongrowing cells." *Science*, vol. 343, no. 6174, p. 1245114, Feb. 2014.

[44] T. J. Ford and P. A. Silver, "Synthetic biology expands chemical control of microorganisms," *Current Opinion in Chemical Biology*, vol. 28, pp. 20–28, Oct. 2015.

[45] N. Jagmann and B. Philipp, "Reprint of Design of synthetic microbial communities for biotechnological production processes." *Journal of biotechnology*, vol. 192 Pt B, pp. 293–301, Dec. 2014.

[46] W. Shou, S. Ram, and J. M. G. Vilar, "Synthetic cooperation in engineered yeast populations." *Proceedings of the National Academy of Sciences of the United States of America*, vol. 104, no. 6, pp. 1877–82, Mar. 2007.

[47] H. Youk and W. A. Lim, "Secreting and sensing the same molecule allows cells to achieve versatile social behaviors." *Science*, vol. 343, no. 6171, p. 1242782, Feb. 2014.

[48] C. Conradi and D. Flockerzi, "Switching in Mass Action Networks Based on Linear Inequalities," *SIAM Journal on Applied Dynamical Systems*, vol. 11, no. 1, pp. 110–134, Jan. 2012.

[49] D. Siegal-Gaskins, M. K. Mejia-Guerra, G. D. Smith, and E. Grotewold, "Emergence of switch-like behavior in a large family of simple biochemical networks." *PLoS computational biology*, vol. 7, no. 5, p. e1002039, May 2011.

[50] E. Feliu and C. Wiuf, "A computational method to preclude multistationarity in networks of interacting species." *Bioinformatics*, vol. 29, no. 18, pp. 2327–34, Sept. 2013.

[51] I. Otero-Muras, J. R. Banga, and A. A. Alonso, "Characterizing multistationarity regimes in biochemical reaction networks." *PloS one*, vol. 7, no. 7, p. e39194, Jan. 2012.

[52] J. Ang, E. Harris, B. J. Hussey, R. Kil, and D. R. McMillen, "Tuning response curves for synthetic biology." *ACS synthetic biology*, vol. 2, no. 10, pp. 547–67, Oct. 2013.

[53] J. A. J. Arpino, E. J. Hancock, J. Anderson, M. Barahona, G.-B. V. Stan, A. Papachristodoulou, and K. Polizzi, "Tuning the dials of Synthetic Biology." *Microbiology*, vol. 159, no. Pt 7, pp. 1236–53, July 2013.

[54] R. C. Brewster, D. L. Jones, and R. Phillips, "Tuning promoter strength through RNA polymerase binding site design in Escherichia coli." *PLoS computational biology*, vol. 8, no. 12, p. e1002811, Jan. 2012.

[55] R. G. Egbert and E. Klavins, "Fine-tuning gene networks using simple sequence repeats." *Proceedings of the National Academy of Sciences of the United States of America*, vol. 109, no. 42, pp. 16 817–22, Oct. 2012.

[56] K. E. McGinness, T. a. Baker, and R. T. Sauer, "Engineering controllable protein degradation." *Molecular cell*, vol. 22, no. 5, pp. 701–7, June 2006.

[57] S. Cardinale and A. P. Arkin, "Contextualizing context for synthetic biology–identifying causes of failure of synthetic biological systems." *Biotechnology journal*, vol. 7, no. 7, pp. 856–66, July 2012.

[58] A. Y. Weiße, D. A. Oyarzún, V. Danos, and P. S. Swain, "Mechanistic links between cellular trade-offs, gene expression, and growth," *Proceedings of the National Academy of Sciences*, vol. 112, no. 9, pp. E1038–E1047, 2015.

[59] V. Chubukov, L. Gerosa, K. Kochanowski, and U. Sauer, "Coordination of microbial metabolism." *Nature reviews. Microbiology*, vol. 12, no. 5, pp. 327–40, May 2014.

[60] O. Kotte, J. B. Zaugg, and M. Heinemann, "Bacterial adaptation through distributed sensing of metabolic fluxes," *Molecular Systems Biology*, vol. 6, p. 355, Mar. 2010.

[61] P. Xu, W. Wang, L. Li, N. Bhan, F. Zhang, and M. A. G. Koffas, "Design and Kinetic Analysis of a Hybrid Promoter–Regulator System for Malonyl-CoA Sensing in Escherichia coli," *ACS Chemical Biology*, vol. 9, no. 2, pp. 451–458, feb 2014.

[62] J. Kuntz, D. Oyarzún, and G.-B. Stan, "Model Reduction of Genetic-Metabolic Networks via Time Scale Separation," in *A Systems Theoretic Approach to Systems and Synthetic Biology I: Models and System Characterizations*. Springer, 2014, pp. 181–210.

[63] A. Dhooge, W. Govaerts, and Y. A. Kuznetsov, "MATCONT: A MATLAB package for numerical bifurcation analysis of ODEs," *ACM Transactions on Mathematical Software*, vol. 29, no. 2, pp. 141–164, June 2003.

# Supplementary material

## "Design of a bistable switch to control cellular uptake"

By Diego A. Oyarzún[1] and Madalena Chaves[2]

Here we explain: a) how to determine the *bistable regimes* for the uptake circuits (Fig. 2 of the main text); b) how to determine the conditions on the promoter dynamic ranges for bistability (the *design spaces* in Fig. 3–4 of the main text); c) how to determine the conditions for hysteresis in the AR circuit (the inequalities in (19) of the main text). The general model for the uptake circuit is

$$\frac{\mathrm{d}s}{\mathrm{d}t} = g_1(s_0)e_1 - g_2(s)e_2, \tag{S1}$$

$$\begin{aligned}\frac{\mathrm{d}e_1}{\mathrm{d}t} &= \kappa_1^0 + \kappa_1^1\sigma_1(s) - \gamma_1 e_1,\\ \frac{\mathrm{d}e_2}{\mathrm{d}t} &= \kappa_2^0 + \kappa_2^1\sigma_2(s) - \gamma_2 e_2,\end{aligned} \tag{S2}$$

where $(s, e_1, e_2)$ are the concentrations of the metabolite, transport enzyme and utilization enzyme, respectively. The parameters $(\kappa_i^0, \kappa_i^1)$ are enzyme expression rates, and $\gamma_i$ is a first order kinetic rate of protein degradation and dilution by cell growth. We assume that:

- The extracellular metabolite $s_0$ is constant.
- The enzyme turnover rates satisfy $g_i(0) = 0$, they are monotonically increasing $\mathrm{d}g_i/\mathrm{d}x > 0$, and they saturate at $g_i^{\text{sat}} = \lim_{x\to\infty} g_i(x) = \sup g_i$.
- The promoter response curves satisfy $\mathrm{d}\sigma_i/\mathrm{d}s > 0$ when the metabolite activates gene expression, and $\mathrm{d}\sigma_i/\mathrm{d}s < 0$ when the metabolite represses expression.

In our model, the promoters control enzyme expression between a baseline concentration ("off") and maximal concentration ("on")

$$E_i^{\text{off}} = \frac{\kappa_i^0}{\gamma_i}, \quad E_i^{\text{on}} = \frac{\kappa_i^0 + \kappa_i^1}{\gamma_i}. \tag{S3}$$

[1]Department of Mathematics, Imperial College London, UK; E-mail: d.oyarzun@imperial.ac.uk
[2]BioCore team, INRIA Sophia Antipolis, France.

The promoter dynamic ranges ($\mu_i$ in equation (4) in the main text) are defined as:

$$\mu_i = \frac{E_i^{\text{on}}}{E_i^{\text{off}}} = \frac{\kappa_i^0 + \kappa_i^1}{\kappa_i^0}, \tag{S4}$$

and the relative dynamic range ($\mu_{12}$ in equation (5) in the main text) as:

$$\mu_{12} = \frac{E_2^{\text{on}}}{E_1^{\text{off}}} = \frac{\kappa_2^0 + \kappa_2^1}{\kappa_1^0}\frac{\gamma_1}{\gamma_2}. \tag{S5}$$

From the definitions in (S3)–(S5), we note the following equivalences:

$$\begin{aligned} E_1^{\text{off}}/E_2^{\text{off}} = \mu_2/\mu_{12}, \quad E_1^{\text{on}}/E_2^{\text{on}} = \mu_1/\mu_{12}, \\ E_1^{\text{on}}/E_2^{\text{off}} = \mu_1\mu_2/\mu_{12}, \quad E_2^{\text{on}}/E_1^{\text{off}} = \mu_{12}. \end{aligned} \tag{S6}$$

Our analysis is based on a separation of time scales and an approximation of the promoter responses $\sigma_i$ by step functions. In the next sections we detail the general methodology: in Section S1 we show how to recast the model as a 2-dimensional piecewise affine system in conic domains. In Section S2 we explain how to identify the bistable regimes in each circuit. In Section S3 we show how to obtain the conditions for bistability. Finally in Section S4 we derive the conditions for hysteresis in the AR circuit.

## S1 Timescale separation and piecewise affine model

Since metabolic dynamics operate in a much shorter time scale than gene expression, we assume that the metabolite is in quasi steady state with respect to the evolution of enzyme concentrations. We can thus take $\mathrm{d}s/\mathrm{d}t \approx 0$ for all $t$ in equation (S1) to get an algebraic equation for the metabolite concentration

$$g_2(s) = g_1(s_0)\frac{e_1}{e_2}. \tag{S7}$$

We can write a reduced version of the complete model (S1)–(S2)

$$\begin{aligned} \frac{\mathrm{d}e_1}{\mathrm{d}t} &= \kappa_1^0 + \kappa_1^1\bar{\sigma}_1(s) - \gamma_1 e_1, \\ \frac{\mathrm{d}e_2}{\mathrm{d}t} &= \kappa_2^0 + \kappa_2^1\bar{\sigma}_2(s) - \gamma_2 e_2, \end{aligned} \tag{S8}$$

where $s$ is the solution of equation (S7) and we have replaced the promoter response curves ($\sigma_i$) by

$$\underline{\text{Activation}} \qquad \bar{\sigma}_i(s) = \begin{cases} 0, & s < \theta_i, \\ 1, & s > \theta_i. \end{cases} \qquad\qquad \underline{\text{Repression}} \qquad \bar{\sigma}_i(s) = \begin{cases} 1, & s < \theta_i, \\ 0, & s > \theta_i. \end{cases} \tag{S9}$$

The model in (S8) is 2-dimensional approximation of the original system in (S1)–(S2). It corresponds to a piecewise affine differential equation in which enzyme expression rates change between slow ($\kappa_i^0$) and fast rates ($\kappa_i^0 + \kappa_i^1$) depending on whether $s < \theta_i$ or $s > \theta_i$. Using the monotonicity of $g_2(s)$ in (S7), we can find one-to-one correspondences between the concentration $s$ and the ratio $e_1/e_2$. Since $g_2$ is an increasing function of $s$, the inequality $s < \theta_i$ implies that $g_2(s) < g_2(\theta_i)$, which after substituting in (S7) leads to the following equivalences

$$s < \theta_i \iff e_2 > \beta_i e_1, \quad s > \theta_i \iff e_2 < \beta_i e_1, \tag{S10}$$

where $\beta_i = g_1(s_0)/g_2(\theta_i)$. We can use the equivalences in (S10) to recast the reduced model in (S8) as a piecewise affine system defined in three conic domains separated by half-lines of the form $e_2 = \beta_i e_1$ (see Fig. S1).

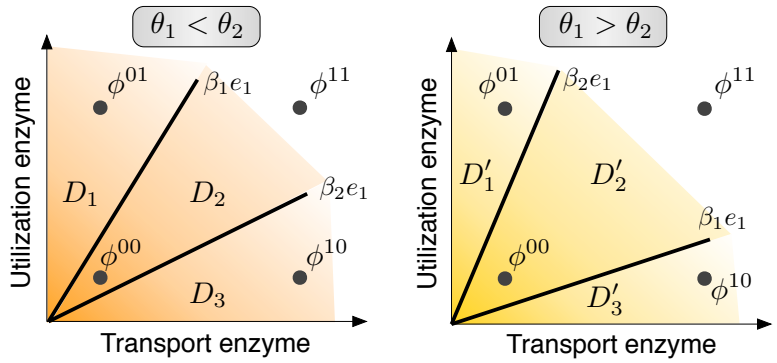


**Figure S1** – State space of the reduced piecewise affine model in (S8). The state space is partitioned in three cones (called $D_k$ if $\theta_1 < \theta_2$, or $D_k'$ if $\theta_1 > \theta_2$ for $k = 1, 2, 3$); the $\beta_i$ parameters are the slopes of the boundary half-lines and defined as $\beta_i = g_1(s_0)/g_2(\theta_i)$. The $\phi^{ij}$ points are defined in Table S1A.

The general form of the piecewise affine ODEs in (S8) is

$$\frac{\mathrm{d}e}{\mathrm{d}t} = \Gamma \left(\phi^{ij} - e\right), \tag{S11}$$

where we defined the concentration vector as $e = (e_1, e_2)^T$, the matrix $\Gamma = \mathrm{diag}\{\gamma_1, \gamma_2\}$, and the $\phi^{ij}$ vectors are combinations of the baseline and maximal expression levels ($E^{\mathrm{off}}$ and $E^{\mathrm{on}}$

given in Table S1A). The vectors $\phi^{ij}$ take different values in different regions of the state space, givein in Table S1B–C. As an example, next we detail the construction of the piecewise affine model for the (R)epression-(R)epression circuit with thresholds ordered as $\theta_1 < \theta_2$.

**Example.** RR circuit with $\theta_1 < \theta_2$.

- If $s < \theta_1$ (or equivalently $e_2 > \beta_1 e_1$), both promoters are in the ON state and thus we can write the right hand side of (S8) as

$$\begin{aligned} \frac{\mathrm{d}e_1}{\mathrm{d}t} &= \gamma_1 \left( \frac{\kappa_1^0 + \kappa_1^1}{\gamma_1} - e_1 \right), \\ \frac{\mathrm{d}e_2}{\mathrm{d}t} &= \gamma_2 \left( \frac{\kappa_2^0 + \kappa_2^1}{\gamma_2} - e_2 \right), \end{aligned} \quad \text{if } e_2 > \beta_1 e_1. \tag{S12}$$

- If $\theta_1 < s < \theta_2$ (or equivalently $\beta_2 e_1 < e_2 < \beta_1 e_1$), promoter 1 is in the OFF state, and promoter 2 in the ON state, thus we can write the right hand side of (S8) as

$$\begin{aligned} \frac{\mathrm{d}e_1}{\mathrm{d}t} &= \gamma_1 \left( \frac{\kappa_1^0}{\gamma_1} - e_1 \right), \\ \frac{\mathrm{d}e_2}{\mathrm{d}t} &= \gamma_2 \left( \frac{\kappa_2^0 + \kappa_2^1}{\gamma_2} - e_2 \right), \end{aligned} \quad \text{if } \beta_2 e_1 < e_2 < \beta_1 e_1. \tag{S13}$$

- If $s > \theta_2$ (or equivalently $e_2 < \beta_2 e_1$) both promoters are in the OFF state, and thus we can write the right hand side of (S8) as

$$\begin{aligned} \frac{\mathrm{d}e_1}{\mathrm{d}t} &= \gamma_1 \left( \frac{\kappa_1^0}{\gamma_1} - e_1 \right), \\ \frac{\mathrm{d}e_2}{\mathrm{d}t} &= \gamma_2 \left( \frac{\kappa_2^0}{\gamma_2} - e_2 \right), \end{aligned} \quad \text{if } e_2 < \beta_2 e_1. \tag{S14}$$

We can write equations (S12)–(S14) in vector form and substitute the definitions of $E_i^{\text{off}}$ and $E_i^{\text{on}}$ (shown in (S3)) to get:

$$\frac{\mathrm{d}e}{\mathrm{d}t} = \begin{cases} \Gamma \left( \phi^{11} - e \right), \text{ if } e \in D_1, \\ \Gamma \left( \phi^{01} - e \right), \text{ if } e \in D_2, \\ \Gamma \left( \phi^{00} - e \right), \text{ if } e \in D_3, \end{cases} \tag{S15}$$

The conic domains $D_i$ are defined in Table S1B and illustrated in Fig. S1; the RR case in (S15) corresponds to the first row of Table S1B.

**Table S1** – Piecewise affine description of the timescale-separated model in (S8). (**A**) Possible stable steady states for the transport and utilization enzymes. (**B**) Piecewise affine models with $\theta_1 < \theta_2$; the RR row corresponds to the example in equations (S12)–(S14). (**C**) Piecewise affine models with $\theta_1 > \theta_2$.

**A**

| Steady state | Transport ($e_1$) | Utilization ($e_2$) |
|---|---|---|
| $\phi^{00}$ | $E_1^{\text{off}}$ | $E_2^{\text{off}}$ |
| $\phi^{01}$ | $E_1^{\text{off}}$ | $E_2^{\text{on}}$ |
| $\phi^{10}$ | $E_1^{\text{on}}$ | $E_2^{\text{off}}$ |
| $\phi^{11}$ | $E_1^{\text{on}}$ | $E_2^{\text{on}}$ |

**B**

| | $\theta_1 < \theta_2$ | | |
|---|---|---|---|
| Circuit | Domain $D_1$ $e_2 > \beta_1 e_1$ | Domain $D_2$ $\beta_2 e_1 < e_2 < \beta_1 e_1$ | Domain $D_3$ $e_2 < \beta_2 e_1$ |
| RR | $\dot{e} = \Gamma\left(\phi^{11} - e\right)$ | $\dot{e} = \Gamma\left(\phi^{01} - e\right)$ | $\dot{e} = \Gamma\left(\phi^{00} - e\right)$ |
| AA | $\dot{e} = \Gamma\left(\phi^{00} - e\right)$ | $\dot{e} = \Gamma\left(\phi^{10} - e\right)$ | $\dot{e} = \Gamma\left(\phi^{11} - e\right)$ |
| AR | $\dot{e} = \Gamma\left(\phi^{01} - e\right)$ | $\dot{e} = \Gamma\left(\phi^{11} - e\right)$ | $\dot{e} = \Gamma\left(\phi^{10} - e\right)$ |

**C**

| | $\theta_1 > \theta_2$ | | |
|---|---|---|---|
| Circuit | Domain $D_1'$ $e_2 > \beta_2 e_1$ | Domain $D_2'$ $\beta_1 e_1 < e_2 < \beta_2 e_1$ | Domain $D_3'$ $e_2 < \beta_1 e_1$ |
| RR | $\dot{e} = \Gamma\left(\phi^{11} - e\right)$ | $\dot{e} = \Gamma\left(\phi^{10} - e\right)$ | $\dot{e} = \Gamma\left(\phi^{00} - e\right)$ |
| AA | $\dot{e} = \Gamma\left(\phi^{00} - e\right)$ | $\dot{e} = \Gamma\left(\phi^{01} - e\right)$ | $\dot{e} = \Gamma\left(\phi^{11} - e\right)$ |
| AR | $\dot{e} = \Gamma\left(\phi^{01} - e\right)$ | $\dot{e} = \Gamma\left(\phi^{00} - e\right)$ | $\dot{e} = \Gamma\left(\phi^{10} - e\right)$ |

# S2 Identification of the bistable regimes.

In this section we show how to obtain the bistable regimes in Fig. 2 of the main text. We first show how to obtain the steady state enzyme concentrations and how to guarantee the existence of a steady state metabolite concentration, without computing its value. Later in Section S3 we derive parametric conditions for bistability, which we then use to determine the qualitative value of the metabolite concentration (i.e. the "low", "intermediate" and "high" concentration metabolite levels in Fig. 2 of the main text).

## S2.1 Steady state enzyme concentrations

We obtain the stable steady state enzyme concentrations by imposing conditions on the $\phi^{ij}$ vectors in the piecewise affine models in (S11). The key observation is that a point $\phi^{ij}$ is a locally stable steady state of the piecewise affine system if and only if it belongs to its corresponding domain. Therefore, for a circuit to have two stable steady states, we need to ensure that at least

two points $\phi^{ij}$ belong to their conic domain. To guarantee that those steady states lead to a bistable uptake flux, they should have different values for the $e_1$ coordinate (recall from equation (6) in the main text, that the flux is proportional to the transport enzyme, i.e. $J = g_1(s_0)\bar{e}_1$). We illustrate this idea with an example.

**Example.** RR circuit with $\theta_1 < \theta_2$.
From Table S1B we see that the RR circuit with $\theta_1 < \theta_2$ can lead to a bistable flux in three cases:

- $\phi^{11} \in D_1$ and $\phi^{00} \in D_3$.
- $\phi^{11} \in D_1$ and $\phi^{01} \in D_2$.
- $\phi^{11} \in D_1$, $\phi^{01} \in D_2$ and $\phi^{00} \in D_3$.

Note that a fourth case, $\phi^{01} \in D_2$ and $\phi^{00} \in D_3$, can be ruled out because $e_1$ is at a low concentration in both $\phi^{01}$ and $\phi^{00}$, and therefore these two steady states would not lead to a bistable flux.

With the above idea we can single out all the possible bistable regimes for each circuit. In Table S2 we have detailed all the conditions on the $\phi^{ij}$ vectors for each regime; in particular, the example (RR case with $\theta_1 < \theta_2$) corresponds to regimes RR-0, RR-2 and RR-4 in Table S2. In Table S2 there are a total of 15 possible arrangements of vectors $\phi^{ij}$ and conic domains that lead to a bistable flux. Note, however, that six of these regimes are infeasible in the sense that the conditions for bistability cannot be met for any combination of positive parameters (marked in red in Table S2). The infeasibility of these regimes can be readily checked from the conditions in Table S2 and the geometry of the state space in Fig. S1. The nine remaining regimes are the ones reported in Fig. 2 of the main text.

## S2.2 Existence of the steady state metabolite concentration.

The steady state for the metabolite satisfies the equation in (S7):

$$g_2(\bar{s}) = g_1(s_0)\frac{\bar{e}_1}{\bar{e}_2}. \tag{S16}$$

However, because $g_2$ saturates at $g_2^{\text{sat}}$, equation (S16) may not have a solution for every $(\bar{e}_1, \bar{e}_2)$ pair. To guarantee that $g_2(\bar{s}) < g_2^{\text{sat}}$, and therefore the existence of a steady state concentration for the metabolite, we need the steady state enzyme concentrations to satisfy

$$\bar{e}_2 > \frac{g_1(s_0)}{g_2^{\text{sat}}}\bar{e}_1 = \check{\beta}\bar{e}_1, \tag{S17}$$

**Table S2** – Bistable regimes in each uptake circuit. The regimes in red are infeasible, as the conditions cannot be met with any combination of parameters (due to the geometry of the state space, see Fig. S1). The feasible regimes are those shown in Fig. 2 of the main text. The crosses indicate the threshold-dependent regimes, i.e. those that emerge only under specific orderings of the thresholds.

| Regime | $\theta_1 < \theta_2$ | $\theta_1 > \theta_2$ |
|---|---|---|
| RR-0 | $\phi^{11} \in D_1, \phi^{00} \in D_3$ | $\phi^{11} \in D'_1, \phi^{00} \in D'_3$ |
| RR-1 | × | $\phi^{10} \in D'_2, \phi^{00} \in D'_3$ |
| RR-2 | $\phi^{11} \in D_1, \phi^{01} \in D_2$ | × |
| RR-3 | × | $\phi^{11} \in D'_1, \phi^{10} \in D'_2, \phi^{00} \in D'_3$ |
| RR-4 | $\phi^{11} \in D_1, \phi^{01} \in D_2, \phi^{00} \in D_3$ | × |
| AA-0 | $\phi^{00} \in D_1, \phi^{11} \in D_3$ | $\phi^{00} \in D'_1, \phi^{11} \in D'_3$ |
| AA-1 | × | $\phi^{01} \in D'_2, \phi^{11} \in D'_3$ |
| AA-2 | $\phi^{00} \in D_1, \phi^{10} \in D_2$ | × |
| AA-3 | × | $\phi^{00} \in D'_1, \phi^{01} \in D'_2, \phi^{11} \in D'_3$ |
| AA-4 | $\phi^{00} \in D_1, \phi^{10} \in D_2, \phi^{11} \in D_3$ | × |
| AR-0 | $\phi^{01} \in D_1, \phi^{10} \in D_3$ | $\phi^{01} \in D'_1, \phi^{10} \in D'_3$ |
| AR-1 | × | $\phi^{00} \in D'_2, \phi^{10} \in D'_3$ |
| AR-2 | × | $\phi^{01} \in D'_1, \phi^{00} \in D'_2, \phi^{10} \in D'_3$ |
| AR-3 | $\phi^{01} \in D_1, \phi^{11} \in D_2$ | × |
| AR-4 | $\phi^{01} \in D_1, \phi^{11} \in D_2, \phi^{10} \in D_3$ | × |

where $\check{\beta} = g_1(s_0)/g_2^{\text{sat}}$. Although the exact steady state metabolite concentration can be computed from the equation in (S16), for our purposes it is more useful to determine its concentration relative to the regulatory thresholds $\theta_1$ and $\theta_2$. This allows us to distinguish between different bistable regimes based on the qualitative value of the metabolite concentration. For example, in the case $\theta_1 < \theta_2$, we can classify the metabolite concentration as "low" when $\bar{s} < \theta_1$, "intermediate" when $\theta_1 < \bar{s} < \theta_2$, and "high" when $\bar{s} > \theta_2$. As we show in the next section, we can deduce the qualitative value of the metabolite concentration from the conditions for bistability.

## S3 Parametric conditions for bistability

From the ideas in Section S2, we can summarize a general procedure to obtain analytic conditions for bistability:

1. For a given bistable regime in Table S2, impose the conditions for local stability $\phi^{ij} \in D_k$ using the definitions in Table S1.

2. For each stable steady state, impose the condition for existence of the metabolite steady state,

i.e. $e_2 > \check{\beta} e_1$ in (S17).

3. Rewrite the conditions in terms of the promoter dynamic ranges $\mu_1$, $\mu_2$ and $\mu_{12}$ using the relations in (S6).

4. Discard any redundant inequalities.

5. Determine the qualitative value of the steady state metabolite concentration by using (S16) for each steady state and combining it with the derived inequalities.

Using the above steps in each of regimes in Table S2 we get the conditions for bistability detailed in Table S3 and Fig. 3–4 of the main text. To illustrate the application of steps 1-5 above, we show the full calculations in detail for two representative cases: the AA-2 regime and the AR-0 regime. These two examples are representative of the general procedure and contain all the elements needed to obtain the conditions for bistability in Table S3.

**Example 1:** AA-2 regime.

1. Following Table S2, we can guarantee the existence of two stable enzyme steady states by enforcing the following conditions

$$\phi^{00} \in D_1, \text{ and } \phi^{10} \in D_2, \tag{S18}$$

which using the definitions in Table S1A become

$$E_2^{\text{off}} > \beta_1 E_1^{\text{off}}, \text{ and } \beta_2 E_1^{\text{on}} < E_2^{\text{off}} < \beta_1 E_1^{\text{on}}. \tag{S19}$$

2. To guarantee the existence of a steady state for the metabolite, we impose condition (S17) to each steady state in this regime (i.e. $\phi^{00}$ and $\phi^{10}$)

$$E_2^{\text{off}} > \check{\beta} E_1^{\text{off}}, \text{ and } E_2^{\text{off}} > \check{\beta} E_1^{\text{on}}. \tag{S20}$$

3. Using the equivalences in (S6), we can rewrite conditions (S19)–(S20) in terms of the dynamic ranges:

$$E_2^{\text{off}} > \beta_1 E_1^{\text{off}} \iff \mu_{12} > \beta_1 \mu_2, \tag{S21}$$

$$\beta_2 E_1^{\text{on}} < E_2^{\text{off}} < \beta_1 E_1^{\text{on}} \iff \beta_2 \mu_1 \mu_2 < \mu_{12} < \beta_1 \mu_1 \mu_2, \tag{S22}$$

$$E_2^{\text{off}} > \check{\beta} E_1^{\text{off}} \iff \mu_{12} > \check{\beta} \mu_2, \tag{S23}$$

$$E_2^{\text{off}} > \check{\beta} E_1^{\text{on}} \iff \mu_{12} > \check{\beta} \mu_1 \mu_2. \tag{S24}$$

4. The conditions (S21)–(S24) can be put together as in Table S3. Note that the inequalities (S23)–(S24) are redundant because $\check{\beta} < \beta_2 < \beta_1$ (recall that $\theta_1 < \theta_2$ in the AA-2 regime) and thus the inequalities in (S21)–(S22) imply that both (S23)–(S24) are automatically satisfied.

5. To determine the location of the metabolite steady state, we substitute $\phi^{00}$ in equation (S16) to obtain

$$g_2(\bar{s}) = g_1(s_0)\frac{E_1^{\text{off}}}{E_2^{\text{off}}} = g_1(s_0)\frac{\mu_2}{\mu_{12}}, \tag{S25}$$

but from the condition in (S21) we know that $\mu_{12} > \beta_1\mu_2 = (g_1(s_0)/g_2(\theta_1))\,\mu_2$, which after substituting in (S25) leads to

$$g_2(\bar{s}) < g_2(\theta_1). \tag{S26}$$

By monotonicity of $g_2$ we conclude that that $\bar{s} < \theta_1$, and thus the steady state $\phi^{00}$ leads to a low steady state concentration for the metabolite.

Conversely, substituting the steady state $\phi^{10}$ in equation (S16) leads to

$$g_2(\bar{s}) = g_1(s_0)\frac{E_1^{\text{on}}}{E_2^{\text{off}}} = g_1(s_0)\frac{\mu_1\mu_2}{\mu_{12}}, \tag{S27}$$

but from the condition in (S22) we know that $\beta_2\mu_1\mu_2 < \mu_{12} < \beta_1\mu_1\mu_2$, or more explicitly

$$\frac{g_1(s_0)}{g_2(\theta_2)}\mu_1\mu_2 < \mu_{12} < \frac{g_1(s_0)}{g_2(\theta_1)}\mu_1\mu_2, \tag{S28}$$

which after substituting in (S27) leads to

$$g_2(\theta_1) < g_2(\bar{s}) < g_2(\theta_2). \tag{S29}$$

Monotonicity of $g_2$ implies that $\theta_1 < \bar{s} < \theta_2$ and thus the steady state state $\phi^{10}$ corresponds to an intermediate metabolite steady state concentration.

**Example 2:** AR-0 regime.

1. Without loss of generality, here we assume that $\theta_1 > \theta_2$ but the same analysis can be done for the converse case. Following Table S2, we can guarantee the existence of two stable enzyme steady states by enforcing the following conditions

$$\phi^{01} \in D_1', \text{ and } \phi^{10} \in D_3', \tag{S30}$$

which using the definitions in Table S1A become

$$E_2^{\text{on}} > \beta_2 E_1^{\text{off}}, \text{ and } E_2^{\text{off}} < \beta_1 E_1^{\text{on}}. \tag{S31}$$

2. To guarantee the existence of a steady state for the metabolite, we impose condition (S17) to each steady state in this regime (i.e. $\phi^{01}$ and $\phi^{10}$)

$$E_2^{\text{on}} > \check{\beta} E_1^{\text{off}}, \text{ and } E_2^{\text{off}} > \check{\beta} E_1^{\text{on}}. \tag{S32}$$

3. Using the equivalences in (S6), we can rewrite conditions (S31)–(S32) in terms of the dynamic ranges:

$$E_2^{\text{on}} > \beta_2 E_1^{\text{off}} \iff \mu_{12} > \beta_2, \tag{S33}$$
$$E_2^{\text{off}} < \beta_1 E_1^{\text{on}} \iff \mu_{12} < \beta_1 \mu_1 \mu_2, \tag{S34}$$
$$E_2^{\text{on}} > \check{\beta} E_1^{\text{off}} \iff \mu_{12} > \check{\beta}, \tag{S35}$$
$$E_2^{\text{off}} > \check{\beta} E_1^{\text{on}} \iff \mu_{12} > \check{\beta} \mu_1 \mu_2. \tag{S36}$$

4. The conditions (S33)–(S36) can be put together as in Table S3. Note that the inequality (S35) is redundant because $\check{\beta} < \beta_2$ and thus (S33) implies that (S35) is automatically satisfied.

5. To determine the location of the metabolite steady state, we substitute $\phi^{01}$ in equation (S16) we obtain

$$g_2(\bar{s}) = g_1(s_0)\frac{E_1^{\text{off}}}{E_2^{\text{on}}} = \frac{g_1(s_0)}{\mu_{12}}, \tag{S37}$$

but from the condition in (S33) we know that $\mu_{12} > \beta_2 = g_1(s_0)/g_2(\theta_2)$, which after substituting in (S37) leads to

$$g_2(\bar{s}) < g_2(\theta_2). \tag{S38}$$

By monotonicity of $g_2$ we conclude that that $\bar{s} < \theta_2$, and thus the steady state $\phi^{01}$ leads to a low steady state concentration for the metabolite.

Conversely, substituting the steady state $\phi^{10}$ in equation (S16) leads to

$$g_2(\bar{s}) = g_1(s_0)\frac{E_1^{\text{on}}}{E_2^{\text{off}}} = g_1(s_0)\frac{\mu_1\mu_2}{\mu_{12}}, \tag{S39}$$

but from the condition in (S34) we know that $\mu_{12} < \beta_1\mu_1\mu_2 = (g_1(s_0)/g_2(\theta_1))\mu_1\mu_2$, which

after substituting in (S39) leads to

$$g_2(\bar{s}) > g_2(\theta_1). \tag{S40}$$

which by monotonicity implies that $\bar{s} > \theta_1$ and thus the steady state $\phi^{10}$ corresponds to a high metabolite steady state concentration.

**Table S3** – Conditions for bistability in each regime. The parameters are $\beta_i = g_1(s_0)/g_2(\theta_i)$. The crosses indicate the threshold-dependent regimes, i.e. those that emerge only under specific orderings of the thresholds. The conditions for the threshold-independent regimes are depicted in Fig. 3 of the main text; the conditions for the threshold-dependent regimes are shown in Fig. 4.

| Regime | $\theta_1 < \theta_2$ | $\theta_1 > \theta_2$ |
|---|---|---|
| RR-0 | $\beta_1\mu_1 < \mu_{12} < \beta_2\mu_2$<br>$\check{\beta}\mu_2 < \mu_{12}$ | $\beta_2\mu_1 < \mu_{12} < \beta_1\mu_2$<br>$\check{\beta}\mu_2 < \mu_{12}$ |
| AA-0 | $\beta_1\mu_2 < \mu_{12} < \beta_2\mu_1$<br>$\check{\beta}\mu_1 < \mu_{12}$ | $\beta_2\mu_2 < \mu_{12} < \beta_1\mu_1$<br>$\check{\beta}\mu_1 < \mu_{12}$ |
| AA-1 | × | $\beta_1 < \mu_{12} < \beta_2$<br>$\check{\beta}\mu_1 < \mu_{12} < \beta_1\mu_1$ |
| AA-2 | $\beta_1\mu_2 < \mu_{12} < \beta_1\mu_1\mu_2$<br>$\beta_2\mu_1\mu_2 < \mu_{12}$ | × |
| AR-0 | $\beta_1 < \mu_{12} < \beta_2\mu_1\mu_2$<br>$\check{\beta}\mu_1\mu_2 < \mu_{12}$ | $\beta_2 < \mu_{12} < \beta_1\mu_1\mu_2$<br>$\check{\beta}\mu_1\mu_2 < \mu_{12}$ |
| AR-1 | × | $\beta_1\mu_2 < \mu_{12} < \beta_2\mu_2$<br>$\check{\beta}\mu_1\mu_2 < \mu_{12} < \beta_1\mu_1\mu_2$ |
| AR-2 | × | $\beta_2 < \mu_{12} < \beta_1\mu_1\mu_2$<br>$\beta_1\mu_2 < \mu_{12} < \beta_2\mu_2$<br>$\check{\beta}\mu_1\mu_2 < \mu_{12}$ |
| AR-3 | $\beta_2\mu_1 < \mu_{12} < \beta_1\mu_1$<br>$\beta_1 < \mu_{12}$ | × |
| AR-4 | $\beta_1 < \mu_{12} < \beta_1\mu_1$<br>$\beta_2\mu_1 < \mu_{12} < \beta_2\mu_1\mu_2$<br>$\check{\beta}\mu_1\mu_2 < \mu_{12}$ | × |

## S4 Conditions for hysteresis in the AR-0 regime

Here we show the derivation of the conditions in (19c)–(19d) for hysteresis in the Activation-Repression circuit operating in the AR-0 bistable regime. The key idea is to guarantee two

saddle-node-like bifurcations for different values of the $\beta_i$ parameters (and hence different concentrations of extracellular metabolite).

We assume that both promoters have equal regulatory thresholds, i.e. $\theta_1 = \theta_2 = \theta$, as this criterion helps to enlarge the design space for promoter dynamic ranges (recall Fig. 3 in the main text). Note that under equal thresholds, the domains $D_2$ and $D_2'$ in the piecewise affine models of Table S1 collapse, and moreover $D_1 = D_1'$ and $D_3 = D_3'$. We define the parameter

$$\beta(s_0) = \frac{g_1(s_0)}{g_2(\theta)}, \tag{S41}$$

where with a slight abuse of notation we have made the dependence of $\beta$ on the metabolite $s_0$ explicit. Since the transport turnover rate, $g_1$, is a non-decreasing function, $\beta(s_0)$ increases with the concentration $s_0$. We can analyze the bifurcations of the piecewise affine model in Table S1 by fixing the location of the $\phi^{ij}$ points and using the ideas in Example 2 of Section S3 for different values of $\beta(s_0)$. Following the notation in Table S1, to have a bistable hysteretic response we need

$$\text{low flux: } \begin{cases} \phi^{01} \in D_1, \\ \phi^{10} \notin D_3, \end{cases} \quad \text{for } s_0 < s_0^{\text{off}}, \tag{S42}$$

$$\text{bistable flux: } \begin{cases} \phi^{01} \in D_1, \\ \phi^{10} \in D_3, \end{cases} \quad \text{for } s_0^{\text{off}} < s_0 < s_0^{\text{on}}, \tag{S43}$$

$$\text{high flux: } \begin{cases} \phi^{01} \notin D_1, \\ \phi^{10} \in D_3, \end{cases} \quad \text{for } s_0 > s_0^{\text{on}}. \tag{S44}$$

The concentrations $s_0^{\text{off}}$ and $s_0^{\text{on}}$ in the (S42)–(S44) represent the amount of metabolite needed to switch the circuit from a high to low flux and *vice versa*. Note that condition (S42) is naturally satisfied because $g_1(0) = 0$ and therefore we can always find a sufficiently small $s_0^{\text{off}}$ such that $\phi^{10} \notin D_3$ for $s_0 < s_0^{\text{off}}$ (or equivalently $E_2^{\text{off}} > \beta(s_0) E_1^{\text{on}}$ for $s_0 < s_0^{\text{off}}$).

Condition (S43) is identical to the ones in (S30) and therefore it is satisfied provided that the dynamic ranges satisfy the bounds in (S33)–(S34) when $s_0^{\text{off}} < s_0 < s_0^{\text{on}}$.

Condition (S44) can be satisfied if there exists $s_0^{\text{on}}$ such that $\phi^{01} \notin D_1$ for $s_0 > s_0^{\text{on}}$, or equivalently

$$E_2^{\text{on}} < \beta(s_0) E_1^{\text{off}}, \tag{S45}$$

for $s_0 > s_0^{\text{on}}$. A sufficient condition for (S45) to hold for $s_0 > s_0^{\text{on}}$ is that in the saturation limit,

i.e. when $s_0 \to \infty$:

$$E_2^{\text{on}} < \hat{\beta} E_1^{\text{off}}, \tag{S46}$$

where $\hat{\beta} = g_1^{\text{sat}}/g_2(\theta)$. The condition (S46) above corresponds to condition (19c) in the main text.

Finally, we need to guarantee that the metabolite steady state $\bar{s}$ exists for all $s_0 > 0$. Recalling the condition in (S36), we need

$$E_2^{\text{off}} > \frac{g_1(s_0)}{g_2^{\text{sat}}} E_1^{\text{on}}, \text{ for all } s_0 > 0, \tag{S47}$$

Since $g_1$ saturates at $g_1^{\text{sat}}$, a sufficient condition for (S47) to hold for all $s_0 > 0$ is

$$E_2^{\text{off}} > \frac{g_1^{\text{sat}}}{g_2^{\text{sat}}} E_1^{\text{on}}, \tag{S48}$$

which corresponds to condition (19d) in the main text.